Journal of South American Earth Sciences 67 (2016) 158–179

Contents lists available at ScienceDirect

Journal of South American Earth Sciences

journal homepage: www.elsevier.com/locate/jsames

Petrology and mineralogy of the La Peña igneous complex, Mendoza, Argentina: An alkaline occurrence in the Miocene magmatism of the Southern Central Andes

Diego Sebastián Pagano [a, b, *], Miguel Ángel Galliski [a], María Florencia Márquez-Zavalía [a, c], Fernando Colombo [d]

[a] IANIGLA, CCT-Mendoza, CONICET, Av. Ruiz Leal s/n (5500), Mendoza, Argentina
[b] CCT-San Luis, CONICET, Departamento de Geología, Universidad Nacional de San Luis, Ejército de los Andes 950, San Luis, 5700, Argentina
[c] Mineralogía y Petrología, FAD, Universidad Nacional de Cuyo, Centro Universitario, 5502, Mendoza, Argentina
[d] CICTERRA-CONICET-FCEFyN-UNC, Av. Vélez Sarsfield 1611, Pab. Geol., X5016CGA, Córdoba, Argentina

ARTICLE INFO

Article history:
Received 23 October 2015
Received in revised form
16 February 2016
Accepted 25 February 2016
Available online 27 February 2016

Keywords:
Alkaline
Potassic
Miocene
Central Andes
Tephrite
Clinopyroxenite

ABSTRACT

The La Peña alkaline igneous complex (LPC) is located in the Precordillera (32°41′34″ S - 68°59′48″ W) of Mendoza province, Argentina, above the southern boundary of the present-day flat-slab segment. It is a 19 km^2 and 5 km diameter subcircular massif emplaced during the Miocene (19 Ma) in the Silurian-Devonian Villavicencio Fm. The LPC is composed of several plutonic and subvolcanic intrusions represented by: a cumulate of clinopyroxenite intruded by mafic dikes and pegmatitic gabbroic dikes, isolated bodies of malignite, a central intrusive syenite that develops a wide magmatic breccia in the contact with clinopyroxenite, syenitic and trachytic porphyries, a system of radial and ring dikes of different compositions (trachyte, syenite, phonolite, alkaline lamprophyre, tephrite), and late mafic breccias. The main minerals that form the LPC, ordered according to their abundance, are: pyroxene (diopside, hedenbergite), calcium amphibole (pargasite, ferro-pargasite, potassic-ferro-pargasite, potassic-hastingsite, magnesio-hastingsite, hastingsite, potassic-ferro-ferri-sadanagaite), trioctahedral micas (annite-phlogopite series), plagioclase (*bytownite to oligoclase*), K-feldspar (sanidine and orthoclase), nepheline, sodalite, apatite group minerals (fluorapatite, hydroxylapatite), andradite, titanite, magnetite, spinel, ilmenite, and several Cu–Fe sulfides. Late hydrothermal minerals are represented by zeolites (scolecite, thomsonite-Ca), epidote, calcite and chlorite.

The trace element patterns, coupled with published data on Sr-Nd-Pb isotopes, suggest that the primary magma of the LPC was generated in an initially depleted but later enriched lithospheric mantle formed mainly by a metasomatized spinel lherzolite, and that this magmatism has a subduction-related signature. The trace elements pattern of these alkaline rocks is similar to other Miocene calc-alkaline occurrences from the magmatic arc of the Southern Central Andes.

Mineral and whole-rock chemical compositions support the interpretation that a first batch of a tephritic magma produced a cumulate of clinopyroxenite (clinopyroxene + magnetite + apatite) and a residual melt that crystallized as malignite at a shallow emplacement level (<5 km). Fractional crystallization in a deep chamber, coupled with rock assimilation, produced successive magma pulses that gave the composite central syenite, the syenitic and trachitic porphyries, and trachytic dikes. The latest rocks (phonolites) reflect an extreme fractionation with Ca, Al and K removal by feldspars. Mingling relationships between tephrites-basanites and trachytes-phonolites, plus compositional variations linked to the reabsorption surface observed in the K-feldspar from the phonolitic dikes, suggest recharge events with local mixing in the late-stages of the LPC evolution.

Abbreviations: LPC, La Peña Complex; PU, Paramillos de Uspallata; CC, Cerros Colorados; IU, Internal Unit; EU, External Unit; APIP, Alto Paranaíba Igneous Province.

* Corresponding author. Present address: Universidad Nacional de San Luis, Ejército de los Andes 950, San Luis, 5700, Argentina.
E-mail addresses: dpagano@mendoza-conicet.gob.ar (D.S. Pagano), galliski@mendoza-conicet.gob.ar (M.Á. Galliski), mzavalia@mendoza-conicet.gob.ar (M.F. Márquez-Zavalía), fosfatos@yahoo.com.ar (F. Colombo).

http://dx.doi.org/10.1016/j.jsames.2016.02.006

The emplacement of the LPC melts at a shallow crustal level was favored by the aperture of extensional NNW-SSE fractures genetically linked to a local brittle shear zone, active at 18–19 Ma during a strong compressional event, that initiated the regime of flat-slab subduction in this part of the Andes.

1. Introduction

Most of the magmatic activity related to the development of the northern part of the southern magmatic arc of the Andes during the Upper Cenozoic belongs to the calc-alkaline series and has been extensively studied because of its importance in the understanding of the magmatic arc evolution of the Andes and its metallogenic significance (e.g., Stern, 1989; Skewes and Stern, 1994; Kay et al., 1999; Kay and Mpodozis, 2001, 2002; Reich et al., 2003; Stern et al., 2010). Instead, the alkaline complexes in this tectonic setting are very scarce and have less economic importance; however, they may have a significant importance for understanding the different magmatic processes that happen in a convergent regime. The importance here is that usually alkaline intrusive and subvolcanic complexes are bound to stable, anorogenic cratons, whereas in our case the alkaline intrusive complex is bound to orogenic processes at cratonic margins. The alkaline complexes are usually small-sized and are complicated because of the wide variety of igneous rocks with a plethora of specific names that contribute to confuse their most important features, such as origin and evolution. The scientific importance of the alkaline igneous complexes lies in their petrography, mineralogy and the petrogenetic processes involved in the genesis of these magmas (Mitchell, 1996). The alkaline complexes are usually similar in morphology, size, composition and tectonic setting. Crustal lineaments and associated faults in rift environments normally control their intrusion, even generating intrusive provinces, as it happens in East Africa (Le Bas, 1977), south of Brazil (Morbidelli et al., 1995), or in the Kola Peninsula, Russia (Kogarko et al., 1995). However, some manifestations have been linked to subduction regimes. Examples of these are the kamafugites of the magmatic Roman province (Boari et al., 2009), the Zippa Mountain, Canada (Coulson et al., 1999) and the leucitites of the Sunda Arc, Indonesia (Edwards et al., 1994). In the context of the Andean orogeny, the La Peña alkaline complex, located in the Mendoza province, Argentina, represents an opportunity to explore petrogenetic processes involved in its genesis, and its relation with the Andean tectonic regime. In this paper we study the origin and magmatic evolution of LPC through the petrography, chemical variations of minerals and whole-rock compositions. We show for the first time the compositional trends of petrogenetic minerals and the composition of accessory and secondary phases from LPC. New whole-rock analyses of major and trace elements are presented, and compared with other magmatic centers from the region. Finally, taking into account published and new data, we propose an alternative evolutionary model for the LPC to the one proposed by Zappettini et al. (2013).

2. Methodology

The cartography was made with ASTER GDEM images and a satellite image obtained with the Stitch Maps software from Google Earth. Polished thin sections were petrographically described and the modal compositions were obtained with a manual point counter using not less than 1200 points per thin section. The classification of the rocks was based in the IUGS diagram (Le Maitre, 2002) complemented for some syenites with the proposal of Mitchell and Platt (1979). Selected thin sections were analyzed with a JEOL JXA-8230 electron microprobe (WDS mode), in LAMARX (Universidad Nacional de Córdoba, Argentina). Analytical conditions were: 1–5 μm beam diameter (10 μm for zeolites), 15 kV acceleration potential, 20 nA beam current (10 nA for zeolites and apatite), and a counting time of 10 s on the peak and 5 s on each background position. Standards were apatite (P and F), rhodonite, wollastonite, anorthoclase or orthoclase (Si), ilmenite (Ti), orthoclase or anorthoclase (Al), chromite (Cr), nickeline (Ni), fayalite (Fe), rhodonite (Mn), wollastonite (Ca), forsterite or MgO (Mg), anorthoclase (Na), orthoclase (K), sanbornite (Ba), celestite (Sr and S), sodalite (Cl), samarskite (Y) and synthetic $REEPO_4$ (La, Ce, Nd). Raw data were processed using the ZAF correction as implemented by the JEOL suite of programs. Amphiboles were classified using the AMPH 2012 2.0 software (Oberti et al., 2012). Whole-rock chemical analyses were performed by Activation Laboratories at Ancaster, Ontario (Canada). Rock powders were fused using a mixture of Li meta and tetraborate, dissolved in nitric acid and then analyzed by ICP-OES (major elements, Sc, Be, V, Ba, Sr, Y, Zr), and ICP-MS (Cr, Co, Ni, Cu, Zn, Ga, As, Rb, Nb, Mo, Ag, In, Sn, Sb, Cs, REE, Hf, Ta, W, Tl, Pb, Bi, Th, U).

3. Geological background

The Puesto La Peña Igneous Complex (sensu Villar and Zappettini, 2000), La Peña (Lucassen et al., 2007), or recently called La Peña Complex (LPC) (Pagano et al., 2014) is located in the eastern border of the Precordillera (32°41′34″ S, 68°59′48″ W) of Mendoza province (Argentina) above the southern boundary of the present-day flat-slab segment developed between 28° and 33° S (Fig. 1A). The Upper Cenozoic arc magmatism, in this part of the southern Central Andes was linked to interactions between the Nazca and South American plates, which produced a large volume of calc-alkaline volcanic rocks principally of basaltic-andesitic, andesitic and dacitic compositions emplaced in Paleozoic to Mesozoic (meta) sedimentary rocks of marine and continental origin, as well as in volcanic and plutonic igneous rocks. Numerous studies documented a spatial link between the geodynamic changes such as slab flattening and geochemical changes in the Cenozoic magmatism in this part of the Andes above the flat-slab segment (Kay et al., 1987, 1991, 1999; Stern, 1989; Kay and Mpodozis, 2001, 2002). These variations were controlled by both the compositions and stress state of the lithosphere from which these magmas originated. Beginning at approximately 22 Ma, the Central Andes were affected by a compressional tectonic phase linked with changes in the subduction geometry of the plates from oblique to orthogonal pattern, which produced crustal shortening and reduced magmatic activity. This led to a period of compressional tectonic regime during the Miocene and tectonic inversion along the flat-slab segment of the Andes (Kay and Mpodozis, 2002).

The beginning of the deformation in the west is shown by the change of low-K tholeiites of the Abanico Formation to calc-alkaline dacites from the El Teniente Volcanic Complex (Kay et al., 2005, 2006), which happened between 21 and 19 Ma ago (Charrier et al., 2002, 2005). The Farellones volcanic arc (Vergara et al.,

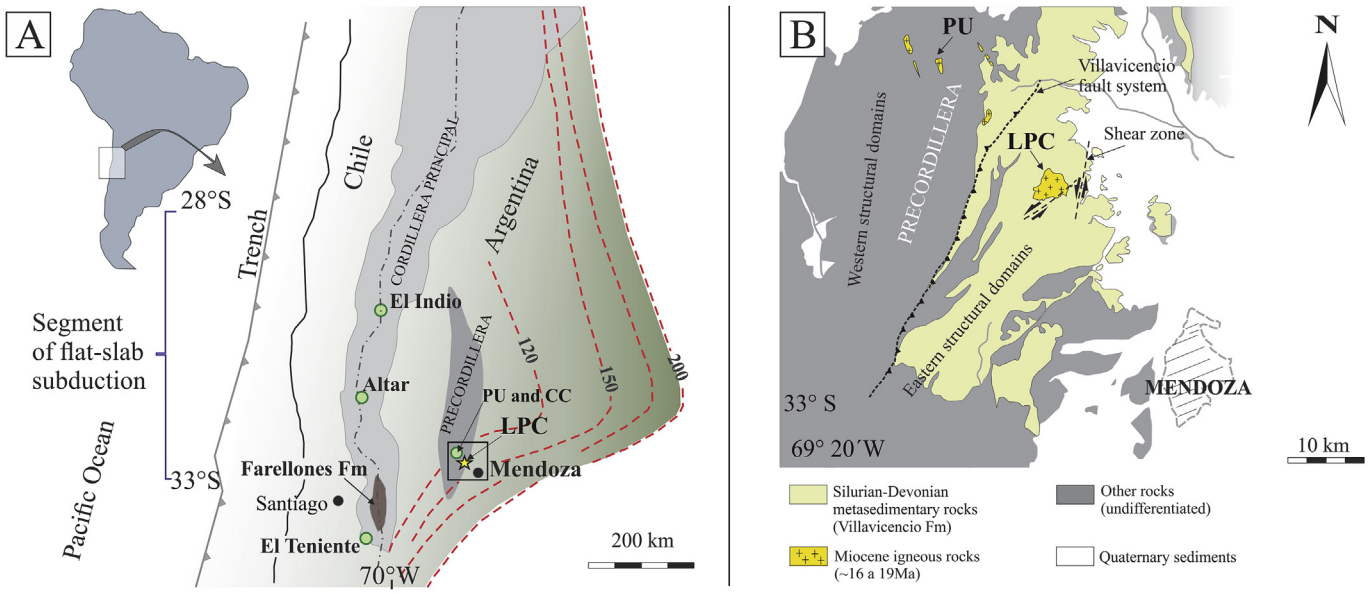

Fig. 1. A) Location of La Peña complex and other Miocene magmatic occurrences in the flat-slab segment, depth contours on the Wadati-Benioff zone from Cahill and Isacks (1992). Figure modified from Kay and Mpodozis (2002). B) Simplified geological map of the southern part of the Precordillera representing the Villavicencio Formation, La Peña complex to the east, and Paramillos de Uspallata westward from Villavicencio fault system. PU: Paramillos de Uspallata, CC: Cerros Colorados.

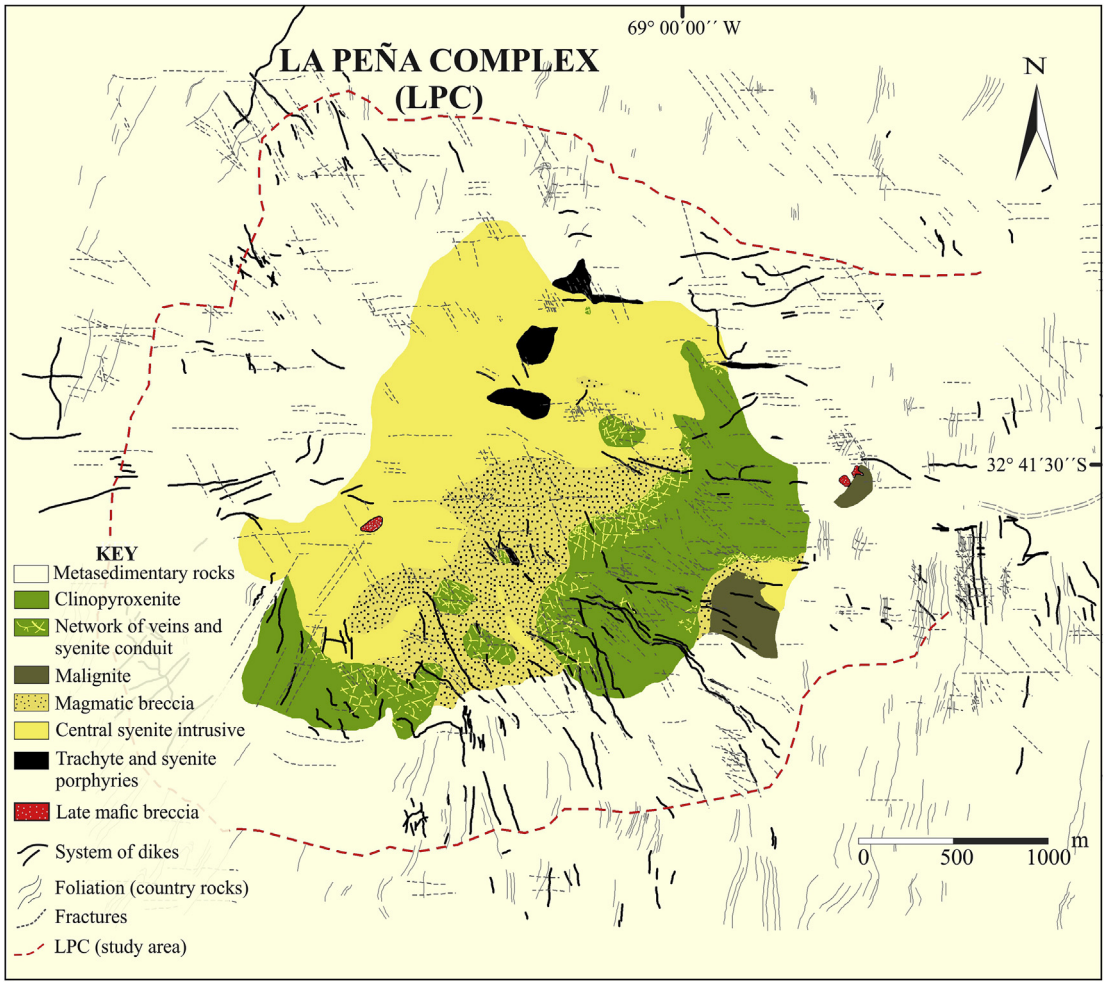

Fig. 2. Geological map of La Peña complex, modified from Pagano et al. (2014).

Table 1
Summary of petrographic characteristics of rocks from the La Peña complex.

Rocks		Mineral compositions	Texture and structure
Clinopyroxenite body	Clinopyroxenite	Cpx > Mag > Ap > Bt ± Pl ± Amp ± Kfs[a]	Medium to coarse grained rock, meso to orthocumular textured.
	Mafic dikes	Cpx > Pl > Kfs > Mag > Bt > Ap	Microporphyritic texture and fluidal structure.
	Mafic dikes	Cpx > Mag > Ap	Fine to very fine grained and fluidal structure.
	Pegmatitic gabbroic dikes	Pl > Amp > Cpx > Mag > Ap > Bt	Large crystals of pargasite in a micropegmatitic groundmass.
Malignite bodies	Malignite (internal unit)[b]	Kfs > Nph > Grt > Cpx > Bt > Amp > Mag > Ttn > Ap > Zr	Heterogeneous, poikilitic, medium to coarse grained texture. Kfs form a poikilitic groundmass including Nph, Cpx, Amp, Bt, Grt, Ttn and Ap.
	Malignite to nepheline syenite (external unit) [c]	Kfs > Nph > Grt > Sdl > Amp > Bt > Mag, Pl > Ttn	Microporphyritic seriate texture and fluidal structure. [d]
Syenite body	Syenite	Kfs > Pl > Amp > Cpx > Mag > Ap > Ttn	Microporphyritic seriate texture.
	Foid syenite	Kfs > Nph > Fd > Cpx > Mag > Ap > Ttn	Microporphyritic seriate texture and fluidal structure.
	Foid monzosyenite	Kfs > Fd > Amp > Pl > Grt > Mag > Ttn > Cpx	Microporphyritic seriate texture and fluidal structure.
	Foid-bearing syenite	Kfs > Pl > Cpx > Fd > Mag > Ttn > Ap	Microporphyritic seriate texture and fluidal structure.
Porphyry bodies	Trachyte porphyries	Kfs > Pl > Cpx > Mag > Ttn > Grt > Ap	Porphyritic texture, and fluidal structure. The phenocrysts (Kfs ± Pl) are contained in a trachytic groundmass.
	Syenite porphyries	Kfs > Pl > Cpx > Fd > Mag > Ttn > Ap	Porphyritic texture, and fluidal structure. The phenocrysts (Pl) are contained in a granular groundmass.
Systems of dikes	Foid-bearing alkali feldspar trachyte	Kfs > Fd > Amp > Cpx > Grt > Mag, Pl > Ttn	Porphyritic texture, and fluidal structure. The phenocrysts (Kfs ± Pl) are contained in a trachytic groundmass (Kfs ± Pl).
	Trachyte	Kfs > Pl > Amp > Mag > Ttn > Cpx	Porphyritic texture, and fluidal structure. The phenocrysts (Pl) are contained in a trachytic groundmass (Kfs ± Pl).
	Syenite	Kfs > Pl > Cpx > Mag > Ttn	Fine grained seriate texture.
	Ledmorite	Kfs > Nph > Grt > Mag > Cpx > Amp, Bt > Ttn > Ap	Fine grained seriate texture.
	Phonolite	Kfs > "Pseudo Lct" > Sdl > Grt > Amp > Pl > Bt > Mag, Cpx >> Ap	Porphyritic texture, and fluidal structure. The phenocrysts are contained in a trachytic groundmass (Kfs ± Pl).
	Phonolite	Kfs > Sdl > Amp > Grt > Pl > Ttn > Mag >> Ap	Porphyritic texture, and fluidal structure. The phenocrysts are contained in a trachytic groundmass (Kfs ± Pl).
	Tephrite	Cpx > Mag > Bt > Ap	Porphyritic to microporphyritic texture, and fluidal structure. The phenocrysts (Cpx, Mag, Bt, Ap) are contained in a very fine grained groundmass (Kfs, Pl, Cpx, Bt, Mag).

References.
[a] Kfs is locally present as an intercumulus phase.
[b] Internal zone of the malignite bodies.
[c] Border zone of malignite bodies; Fd: undifferentiated foid replaced by zeolite; *Pseudo Lct*: pseudoleucite. Other mineral abbreviations are from Whitney and Evans (2010).
More detailed petrographic descriptions in Pagano et al. (2014).

1999), at the base of the Farellones Fm was dated in 22.5 Ma U–Pb (Fock, 2005). To the east, in the back-arc, the Paramillos and Cerro Colorado volcanic centers, with ages of 18.9 to 16.2 Ma (Kay et al., 1991), represent the closest calc-alkaline equivalents (Fig. 1A and B).

3.1. La Peña complex

The studied complex is emplaced in the metasedimentary turbiditic sequence of the Villavicencio Formation (Harrington, 1941) (Fig. 1B), formed by mudstones, sandstones and minor conglomerates of Silurian-Devonian age (Cuerda et al., 1993). This sequence was differentially deformed and slightly metamorphosed during the Chanic diastrophic phase (dated at 385 Ma, Davis et al., 2000), and shows a westward-increasing degree of deformation up to the Villavicencio fault system (Giambiagi et al., 2011). The Villavicencio Formation has to the east, a N–S striking strike-slip brittle shear zone related with the emplacement of the LPC (Pagano et al., 2014) (Fig. 1B).

The LPC is an approximately circular intrusive of 5 km of diameter and 19 km^2 of surface, slightly elongated to the NE–SW direction. It has straight and high-angle contacts with the country rock, concordant with the stratigraphy in the eastern border and discordant to it in the rest of the complex. It is a plutonic, subsaturated, potassic complex, defined as belonging to the malignite-borolanite series (Villar and Zappettini, 2000; Zappettini et al., 2013). The most abundant rock types are clinopyroxenite, malignite and syenite, along with dike swarms of diverse lithologies. An Ar–Ar age in amphibole of the malignite yielded 18.7 ± 0.5 Ma (Zappettini et al., 2005), whereas K/Ar data from amphibole from the clinopyroxenite gave 17.9 ± 0.5, 18.5 ± 0.5, and 19.5 ± 0.6 Ma. An age of 18.8 ± 0.5 Ma was obtained by Lucassen et al. (2007) on biotite of the same rock, confirming that the LCP is an Early Miocene magmatic occurrence. Zappettini et al. (2013) indicated that LPC is formed by two plutonic facies (a pyroxenite core surrounded by a malignite-borolanite association) and a system of radial and annular dikes (trachyte, tephrite to phonolite, alkaline lamprophyre and intermediate varieties, porphyritic microledmorite, benmoreite and alkaline trachyte). Outside of the study area there are also dikes of ouachitite, as well as trachytic to phonolitic volcanic necks. Recently Pagano et al. (2014) published a detailed contribution about the petro-structural aspects of the LPC at meso and microscopic scales; in that paper the authors remarked that the LPC is built by several intrusions (dominantly plutonic; subvolcanic in less proportion) that are grouped in: (1) a clinopyroxenite consisting in a cumulate body intruded by a mafic dike system, and pegmatitic gabbroic dikes, (2) isolated bodies of malignite, (3) a central syenite intrusive with facies of syenite, foid-bearing syenite, foid syenite and monzosyenite producing an intrusive breccia at the contact between clinopyroxenite and syenite, (4) syenitic and trachytic porphyries, and (5) a swarm of radial and ring dikes (Fig. 2) of several compositions that includes: foid-bearing alkali feldspar trachytes, trachytes and, less frequently, syenite, intruded by thin basanitic dikes (now reclassified as tephritic dikes). A more recent geological survey and new petrographic observations allowed to identify the occurrence of scarce

Table 2
Representative modal compositions of rocks from the La Peña complex.

Rocks		n	Cpx	Amp	Bt	Pl	Kfs	Nph	Sdl	PLct[c]	Fd[d]	Ap	Grt	Ttn	Mag	SM
Clinopyroxenite body	Clinopyroxenite	6	76.0	0.1	4.3[a]	2.5[b]	–	–	–	–	–	7.4	–	–	9.8[i]	–
	Mafic dikes[e]	1	55.0	–	1.4	18.3	15.2	–	–	–	–	0.1	–	–	10.0	–
	Mafic dikes[f]	2	71.2	–	–	–	–	–	–	–	–	0.1	–	–	28.7	–
	Pegmatitic g. dikes[g]	3	20.8	23.7	0.9	45.7	–	–	–	–	–	3.5	–	–	4.2	1.2
Malignite bodies	Malignite (internal unit)[h]	4	12.2	9.5	11.6	–	34.0	15.0	–	–	–	0.3	14.0	0.4	1.7[j]	1.3
	Malignite to nepheline syenite (external unit)	2	–	8.0	0.7	0.6	54.5	17.7	1.2	–	–	–	13.9	0.3	0.6	2.5
Syenite body	Syenite	3	4.3	8.7	–	17.6	62.8	0.0	–	–	–	0.7	–	0.6	2.5	2.8
	Foid syenite	2	0.5	6.2	–	–	52.5	18.0	–	–	11.9	–	7.8	0.2	0.9	2.0
	Foid monzosyenite	1	0.2	13.4	–	8.5	55.6	–	–	–	15.0	–	2.4	0.2	0.7	4.1
	Foid-bearing syenite	1	8.3	–	–	16.5	67.5	–	–	–	4.6	0.1	–	0.5	2.5	–
Porphyry bodies	Trachytic porphyries	2	3.2	–	–	18.8	73.2	–	–	–	–	0.2	0.5	0.6	2.0	1.5
	Syenitic porphyries	2	4.1	–	–	14.6	77.2	–	–	–	2.0	0.1	–	0.6	1.4	–
Systems of dikes	Foid-bearing alkali feldspar trachyte	1	3.5	3.7	–	0.8	76.2	–	–	–	8.3	–	2.3	0.1	0.8	4.3
	Trachyte	2	2.1	0.5	–	16.4	71.2	–	–	–	–	–	–	0.7	1.4	7.7
	Syenite	1	6.1	–	–	31.7	59.2	–	–	–	–	–	–	0.6	1.8	0.7
	Ledmorite	1	5.0	2.0	2.0	–	54.3	17.0	–	–	–	0.2	15.7	0.5	1.8	1.5
	Phonolite	1	0.4	3.4	0.5	0.8	67.6	–	7.4	15.4	–	–	4.1	–	0.4	–
	Phonolite	1	–	6.0	–	3.8	72.3	–	12.0	–	–	–	4.8	0.2	0.1	1.0
	Tephrite	1	20.0	–	7.0	[k]	[k]	–	–	–	–	3.0	–	–	15.0	10.0

References: -: not detected; n: number of samples; SM: secondary minerals (zeolites > calcite > epidote, occasional chlorite and possibly cancrinite).
[a] Interstitial late biotite.
[b] Subordinated plagioclase, identified only in one sample of clinopyroxenite.
[c] "pseudoleucite" (pseudomorphs of leucite).
[d] Undifferentiated foid, replaced by zeolite.
[e] Microporphyritic mafic dikes.
[f] Fine grained mafic dikes.
[g] Pegmatitic gabbroic dikes.
[h] In the Internal unit of malignite, zircon was identified by manual separation.
[i] Abundant titanian magnetite, scarce pyrite, chalcopyrite and occasional covellite.
[j] Pyrrhotite + magnetite.
[k] Kfs and Pl forming a very fine grained groundmass. Mineral abbreviations are from Whitney and Evans (2010). Malignite bodies are composed by a heterogeneous rock that in the external unit (border zone) varies from malignite (mesocratic nepheline syenite) to nepheline syenite. Malignite is classified following to IUGS recommendations (Le Maitre, 2002) and the Mitchell and Platt (1979) mineralogical classification.

isolated bodies of late mafic breccias (Fig. 2), and in the systems of dikes the presence of ledmorites, phonolites and alkaline lamprophyric rocks. A summary of the petrographic characteristic of LPC rocks is given in Table 1; the modal composition and mineralogy of different kind of rocks are numerically and graphically shown in Table 2 and Fig. 3.

4. Results

4.1. Chemical composition of the minerals

4.1.1. Pyroxene group minerals

Clinopyroxene is present in diverse proportions, morphology and grain size in most rocks of the LPC. Modal proportion decreases from about 80% in clinopyroxenite, to less than 1% in syenite. In the clinopyroxenite it occurs as 2–30 mm subhedral crystals, whereas in malignite it is much smaller (0.5–1.5 mm). In syenite and trachyte it is frequently replaced by garnet and amphibole. Representative chemical compositions are quoted in Table 3. They correspond to members of the diopside-hedenbergite series in the current IMA classification (Morimoto et al., 1988), although some points show wollastonite (Wo) contents higher than 50% (Fig. 4A). The chemical evolution suggests Fe enrichment by the $Mg_{-1}Fe$ substitution, from clinopyroxenite and tephrite to malignite and syenite. In the $(Fe^{2+}+Mn)$–Na–Mg diagram it can be seen that clinopyroxene from LPC falls in the same field as that from the less evolved rocks from the Magnet Cove alkaline complex, USA (Flohr and Ross, 1990), Ilimaussaq South, Greenland (Larsen, 1976), Coldwell, Canada (Mitchell and Platt, 1982) and Chinduzi, Chilwa, Malawi (Woolley and Platt, 1986) (Fig. 4B).

4.1.2. Calcium amphibole subgroup minerals

The calcium amphibole subgroup minerals occur in most rocks from the LPC in different quantities, from scarce in the clinopyroxenite to 7% in the foid syenite and syenite and up to 12% in the malignite. In the clinopyroxenite they form anhedral crystals up to 5 mm replacing diopside and biotite. In the pegmatitic gabbroic dikes they occur as euhedral to subhedral crystals up to 8 cm long that locally show branching textures. In syenite and malignite, amphibole is usually interstitial or, when filling veinlets, fibrorradial. In trachytic dikes it forms slightly reabsorbed ovoid crystals, while in the phonolitic ones it occurs as up to 5 mm euhedral crystals. Most crystals display a slight to marked concentrical zoning, but all compositions belong to the calcic subgroup. Following the IMA scheme (Hawthorne et al., 2012) they can be classified as pargasite, ferro-pargasite, potassic-ferro-pargasite, hastingsite, magnesio-hastingsite, potassic-hastingsite to potassic-ferro-ferri-sadanagaite. Some representative compositions are listed in Table 4.

Some crystals in phonolitic dikes show homogeneous ovoid cores (ferro-pargasite) wrapped by an outer idiomorphic zone of potassic-ferro-pargasite composition; this compositional contrast between both zones is also marked by K, Al and Ti increase coupled with a decrease in Na and Si.

4.1.3. Mica group minerals

Ferromagnesian micas ("biotite" and phlogopite) are common in the LPC, with modal proportions up to 20% in the clinopyroxenite and 7% in the late tephritic dikes; they are very scarce in the syenites. In clinopyroxenite, biotite is interstitial and represents a late intercumulus phase. Table 5 shows some representative compositions. The $Fe_T/(Fe_T + Mg)$ ratio is variable (between 0.23 and 0.55),

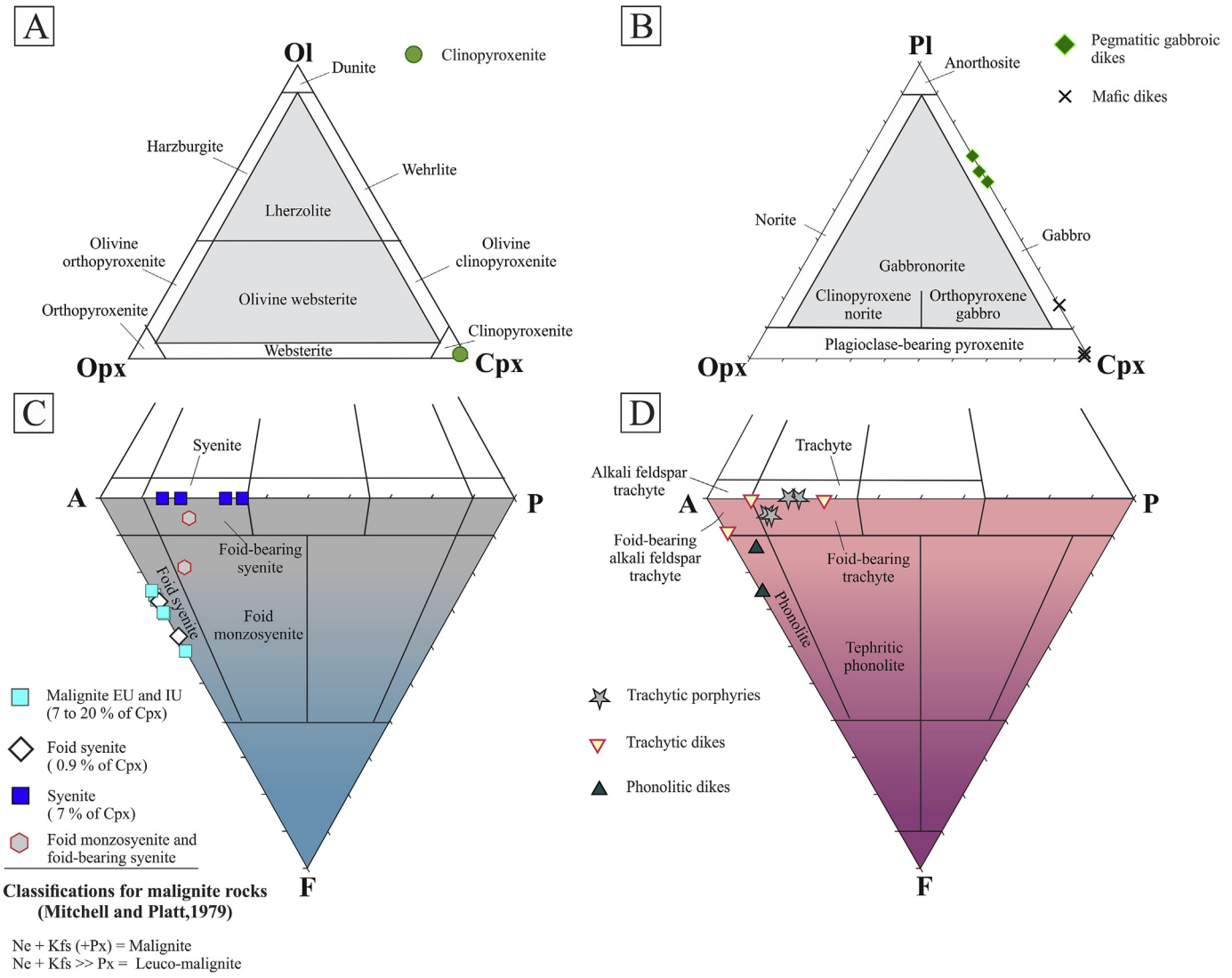

Fig. 3. Diagrams of classification used for LPC rocks based on the recommendations of the IUGS. A) For clinopyroxenite. B) For the gabbroic rocks. C) For the syenitic rocks. It is also shown the mineralogical classification of Mitchell and Platt (1979) for malignites. D) For the volcanic rocks, applied to dikes and porphyries.

and in most cases it is below 0.55 (i.e. they are phlogopite) except locally where annite prevails. These compositions are equivalent to those of micas from the Jacupiranga alkaline complex (Fig. 5A) analyzed by Brod et al. (2001).

4.1.4. K-feldspar

Potassium feldspar is common in LPC rocks, reaching up to 70% in volume in syenite and foid syenite. It occurs as an optically continuous groundmass in the internal unit of the malignite and in the foid syenite, and as intercumulus in the clinopyroxenite. The external unit of the malignite bodies, some foid syenites and syenites have euhedral to subhedral microphenocrysts up to 5 mm in size, whereas in the trachyte and the trachytic phorphyry they can reach up to 5 cm. The chemical compositions (Table 6) are in the range $Or_{54.9}$ $Ab_{42.5}$ $An_{2.6}$ to $Or_{88.6}$ $Ab_{11.4}$ $An_{0.033}$ (Fig. 5B) and the structural state corresponds to sanidine and orthoclase. The contents of minor elements, such as Sr and Ba, show large variations within zoned crystals and among different individuals as well. Some crystals are markedly enriched in Ba (up to 3.86 wt.% BaO) or Sr (up to 3.55 wt.% SrO). In phonolitic dikes crystals show periodic oscillatory zoning, with a sharp increase of Ca, Ba and occasionally Sr after resorption surfaces. These crystals show irregular resorption surfaces but marked idiomorphism in outer zones.

4.1.5. Plagioclase

Plagioclase is relatively abundant as pheno and microphenocryst in syenite, monzosyenite, porphyries, trachytic and phonolitic dikes, and as oriented microlites in the groundmass of trachyte and tephrite. Chemical compositions (Table 6) are variable, ranging between An_{82} (bytownite) and An_{21} (oligoclase) (Fig. 5B), and show good correlation with the magmatic differentiation degree of the LPC rocks.

4.1.6. Nepheline

This is the most abundant foid found in malignite and foid syenite, but it is subordinated to sodalite in phonolitic dikes. It usually occurs as euhedral to subhedral crystals that show the {0001} and {10–10} crystallographic forms. Its chemical composition is quoted in Table 7; the Ne, Ks, Qz and An % *mol* were calculated according to Kononova et al. (1967). In general the compositions are rich in An, with CaO contents varying from 1.34 to 2.48 wt. %, similar to the ones from nepheline monzonite, nepheline diorite and theralite

Table 3
Representative compositions of clinopyroxene from the La Peña complex.

Samples	LP 12 Cpx 1	LP 12 Cpx 1	LP B1 Cpx 1	LP 3c Cpx 3	LP 3c Cpx 3	LP 62 Cpx 2	LP D25 Cpx 1	LP 32D Cpx 2	LP 32D Cpx 1
Rocks	Clinopyroxenite		Mafic dikes	Malignite		Syenite	Phonolitic dikes	Tephritic dikes	
Analysis	5 r	18 c	38 c	66 a	67 a	3 a	31 c	6 c	1 c
SiO_2 wt. %	46.71	50.75	46.63	47.20	46.09	43.37	43.81	50.78	51.01
TiO_2	1.55	0.72	1.65	1.32	1.67	1.54	1.47	0.73	0.77
Al_2O_3	6.62	3.27	7.39	4.84	7.01	7.83	8.16	2.89	3.16
Cr_2O_3	0.05	b.d.l.	0.01	b.d.l.	0.04	0.02	0.04	b.d.l.	b.d.l.
Fe_2O_3	5.31	2.75	5.05	3.99	5.02	7.13	8.46	2.73	2.39
FeO	4.55	3.87	4.90	12.75	5.52	10.46	8.83	3.82	4.75
MnO	0.21	0.13	0.26	0.71	0.21	1.02	0.78	0.09	0.10
MgO	11.30	14.19	10.74	6.29	10.48	5.57	6.05	14.71	14.19
CaO	23.08	23.67	23.61	21.89	23.76	20.80	22.08	23.78	24.05
Na_2O	0.60	0.37	0.58	1.06	0.38	1.12	1.08	0.17	0.15
Total	99.97	99.73	100.83	100.03	100.18	98.84	100.75	99.70	100.59
apfu									
Si	1.756	1.883	1.741	1.832	1.739	1.709	1.689	1.884	1.882
Al(4)	0.244	0.117	0.259	0.168	0.261	0.291	0.311	0.116	0.118
Σ*T*	2.000	2.000	2.000	2.000	2.000	2.000	2.000	2.000	2.000
Al(6)	0.049	0.026	0.066	0.054	0.050	0.073	0.060	0.011	0.020
Ti	0.044	0.020	0.046	0.039	0.047	0.046	0.042	0.020	0.021
Cr	0.001	0.000	0.000	0.000	0.001	0.001	0.001	0.000	0.000
Fe^{3+}	0.150	0.077	0.142	0.116	0.142	0.211	0.246	0.076	0.066
Fe^{2+}	0.139	0.116	0.152	0.414	0.173	0.343	0.285	0.114	0.141
Mg	0.616	0.760	0.593	0.364	0.585	0.326	0.358	0.779	0.751
Mn	0.000	0.000	0.000	0.013	0.000	0.000	0.018	0.000	0.000
Σ*M*1	1.000	1.000	1.000	1.000	1.000	1.000	1.000	1.000	1.000
Fe^{2+}	0.004	0.004	0.001	0.000	0.001	0.001	0.000	0.005	0.006
Mn	0.007	0.004	0.008	0.010	0.007	0.034	0.008	0.003	0.003
Mg	0.017	0.024	0.004	0.000	0.004	0.001	0.000	0.035	0.029
Ca	0.929	0.941	0.944	0.911	0.961	0.878	0.912	0.945	0.951
Na	0.044	0.027	0.042	0.080	0.028	0.085	0.081	0.012	0.011
Σ*M*2	1.000	1.000	1.000	1.000	1.000	1.000	1.000	1.000	1.000
Wo	50.07	48.94	51.40	50.44	51.45	49.85	50.96	48.38	48.89
En	34.12	40.81	32.54	20.16	31.58	18.59	19.42	41.65	40.15
Fs	15.81	10.25	16.06	29.39	16.97	31.56	29.62	9.97	10.96
Mg#	68.33	79.93	66.96	40.69	65.05	37.06	40.28	80.68	78.55

References: c: core; r: rim; a: aleatory. n.d.: not detected. Formulae based on 6 atoms of oxygen and 4 cations.

from the Messum alkaline complex, Namibia (Blancher et al., 2010). The contents of Qz increase from malignite to foid syenites. In some syenite and phonolites, nepheline accompanied by Kfs (plus analcime and fine-grained muscovite), are pseudomorphically replacing leucite, producing pseudoleucite.

4.1.7. Apatite

Minerals of this group are present in all LPC rocks. Their modal content varies from 8% in clinopyroxenite to 0.1% in trachytes. Chemical compositions (Table 8) range from fluorapatite in most rocks to hydroxylapatite in the tephritic dikes (Fig. 6). The contents of SO_3 are significant, ranging from 0.29 to 1.08 wt.%. This corresponds to medium to high S apatites following the definition of Broderick (2008).

4.1.8. Andradite

Andradite with variable Ti content (3–6 wt.% TiO_2) is a common accessory phase in intermediate and evolved rocks, appearing as euhedral crystals up to 2 mm. Crystals from the internal unit of malignite show anisotropic rims in contact with zeolites. Chemical compositions are quoted in Table 9.

4.1.9. Titanite

This mineral is a frequent accessory phase in leucocratic rocks, occurring as subhedral crystals up to1 mm long. In malignite it is resorbed by garnet. Chemical analyses of titanite from syenite (average of 4 spots) gave (wt.%): SiO_2: 30.0; Ti_2O: 33.7; CaO: 27.9; Al_2O_3: 1.6; Fe_2O_3: 2.0.

4.1.10. Sodalite

Sodalite is frequent in phonolitic dikes as microphenocryst. Its average ($n = 4$) chemical composition is (wt.%): SiO_2: 37.5; Al_2O_3: 31.9; FeO: 0.02; Na_2O: 24.51; CaO: 0.18; K_2O: 0.02; Cl: 7.21 and SO_3: 0.09.

4.1.11. Magnetite

In addition to cumulate layers of restricted extent formed only by magnetite (Zappettini et al., 2008, 2009), this oxide is present in variable proportions, from 13% in the main clinopyroxenite down to 3% in syenite and trachyte. The composition of this phase from tephritic dikes is in average ($n = 7$; wt.%): TiO_2: 7.94; Fe_2O_3: 47.33, FeO: 37.07, Al_2O_3: 4.50, Cr_2O_3: 0.06, MnO; 0.21, MgO: 0.91 and SiO_2: 0.09 (Fe^{2+}/Fe^{3+} ratio calculated after Droop, 1987), corresponding to titanian magnetite. Its composition is similar to that of magnetite from clinopyroxenite analyzed by Zappettini et al. (2009). It shows exsolutions of ilmenite and spinel, and hematite replacement along {111} octahedric planes.

4.1.12. Zeolite group minerals

Locally, minerals of this group are filling veinlets and interstitial

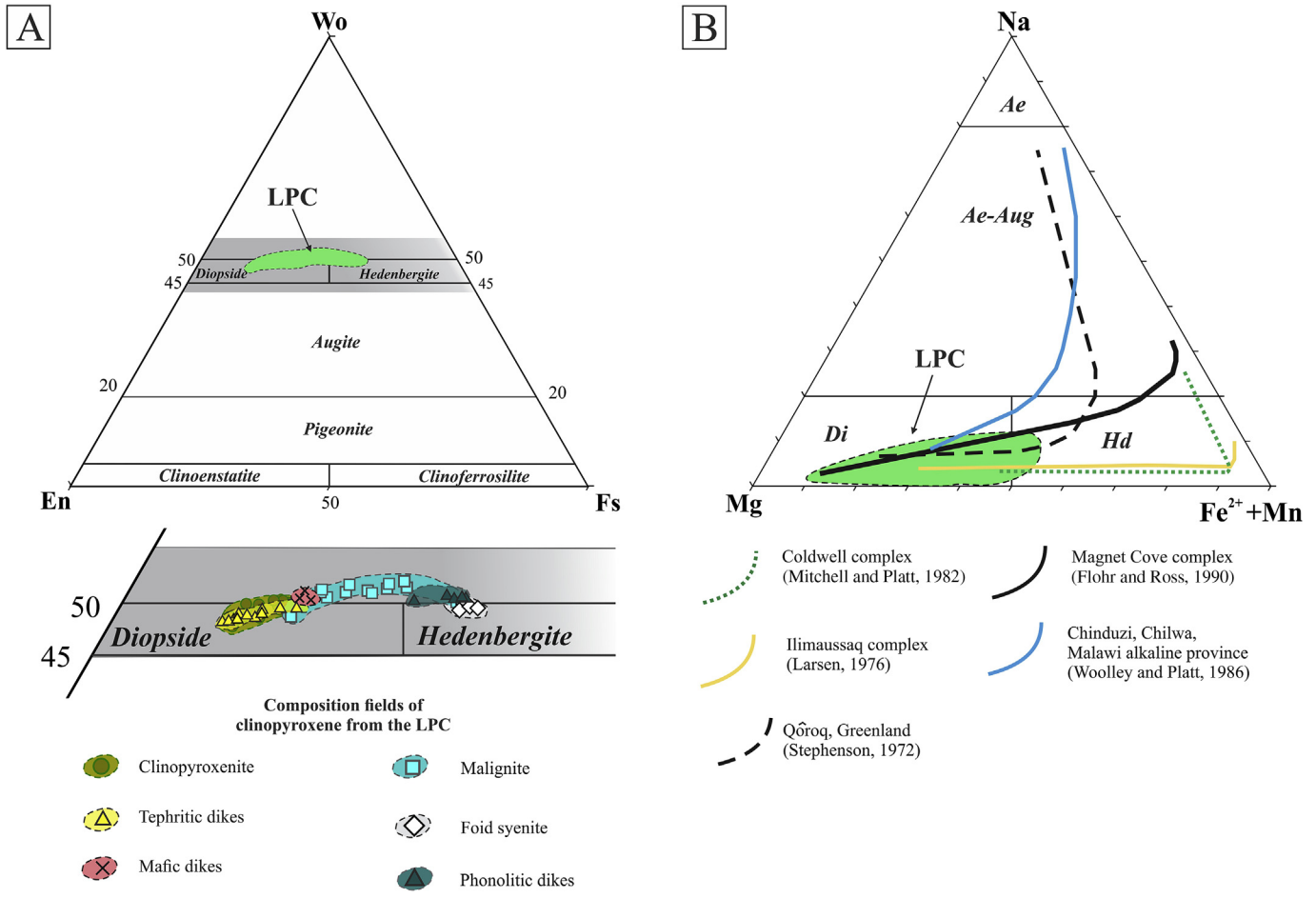

Fig. 4. A) Ternary diagram Ferrosilite (Fs) - Wollastonite (Wo) – Enstatite (En), showing the compositions of the clinopyroxene from LPC following the IMA classification (Morimoto et al., 1988). B) Ternary diagram (Fe^{2+} + Mn) – Na – Mg showing the LPC clinopyroxene compositions compared to the ones from other alkaline complexes: Coldwell (Mitchell and Platt, 1982), Ilimaussaq (Larsen, 1976), Qôroq, Greenland (Stephenson, 1972), Magnet Cove (Flohr and Ross, 1990), Chinduzi, Chilwa, Malawi alkaline province (Woolley and Platt, 1986).

spaces in clinopyroxenite, malignite and syenite. They are also present in pegmatitic differentiates of malignite, as well as replacing nepheline and sodalite. They are high-Ca zeolites, mainly scolecite and thompsonite-Ca. The average chemical composition for scolecite is (n = 12; wt. %): SiO_2: 45.89, Al_2O_3: 25.33, FeO: 0.03, CaO: 12.41, Na_2O: 0.79, K_2O: 0.03, Cl: 0.01, with 13.54% H_2O_{calc}. The thomsonite-Ca composition (wt.%) is: SiO_2: 38.22, Al_2O_3: 30.84, FeO: 0.04, CaO: 12.48, Na_2O: 3.63, K_2O: 0.11, with 13.30H_2O_{calc}.

4.1.13. Other minerals

Zircon is present in small quantities in malignite. Epidote and chlorite group minerals, calcite, and possible some cancrinite locally replace plagioclase, amphibole and nepheline. The first three minerals may also be found filling amygdules and veinlets in trachyte and phonolite dikes. Pyrrhotite, pyrite, chalcopyrite, marcasite and secondary covellite and goethite were observed as sporadic minerals.

4.1.14. Evolution of mineral compositions

Clinopyroxene, biotite, amphibole, feldspars and nepheline chemical compositions show evolutionary trends which are consistent with magmatic differentiation from clinopyroxenite-tephrite-malignite to syenite (trachyte), similar to trends shown in Harker diagrams by whole rock compositions, see below. Clinopyroxene, biotite and amphibole evolved through substitution of Mg by Fe. The Mg# [Mg/(Mg + Fe) *atom.*] in clinopyroxene decreases from 80.06 in diopside from tephritic dikes and clinopyroxenite to 37.06 in hedenbergite from foid syenite. This evolution occurs simultaneously with an increase in Al, Ti and Na (Fig. 7A and B). The decreasing Mg# is coupled with an increase of Al and Ti in single zoned or in different crystals, indicating simple magmatic differentiation operating from tephritic-clinopyroxenite up to malignite.

The enrichment of Na in clinopyroxene from foid syenites and phonolites, and partially in malignite, strongly suggests increasing melt alkalinity with differentiation (Fig. 7B).

Biotite also shows decreasing Mg# with differentiation, from values of 76.57–75.25 in phlogopite from clinopyroxenite and tephritic dikes, to 44.61 in *biotite* from malignite. This behavior is expected if melt evolution was dominated by fractional crystallization, comparable to the chemical evolution of micas in the Jacupiranga alkaline complex (Brod et al., 2001). The FeO_T/Al_2O_3 vs FeO_T/MgO diagram shows Fe enrichment with respect to Al and Mg with differentiation, and a small compositional gap between micas from less evolved rocks compared with the others (Fig. 7C). The Ti content of biotite increases at the beginning with increasing Fe_T/(Fe_T + Mg) in the less differentiated rocks, peaking in mafic dikes and then decreasing towards malignite (Fig. 7D). This initial

Table 4
Representative compositions of amphiboles from the La Peña complex.

Samples	LP	LP	LP	LP	LP	LP	LP	LP	LP
	12	28	8	62	71	D1	D1	D1	D25
	Anf 1	Anf 1	Anf 1	Anf 1	Anf 3	Anf 2	Anf 3	Anf 1	Anf 1
Rocks	Clinopyroxenite	Pgd	Malignite	Foid syenite	Syenite	Trachytic dikes		Phonolitic dikes	
Analysis	1a	3c	21 a	4 c	5a	5 r	6 c	2 c	34 c
SiO_2 wt. %	39.32	38.03	36.73	36.87	40.07	39.63	38.28	39.17	37.72
TiO_2	1.91	2.65	1.76	1.93	0.09	2.33	2.76	3.12	1.68
Al_2O_3	15.15	14.95	13.90	14.10	11.89	13.05	13.77	13.66	13.39
Cr_2O_3	b.d.l.	0.05	b.d.l.	0.03	0.03	0.03	0.05	b.d.l.	0.01
Fe_2O_3	2.06	2.71	3.35	3.97	4.18	1.49	1.20	0.94	3.15
FeO	9.71	10.26	16.92	17.70	14.85	16.53	15.50	15.76	18.64
MnO	0.20	0.22	0.95	1.12	1.81	0.65	0.48	0.42	1.49
MgO	12.75	11.93	6.73	5.97	8.46	8.99	9.06	9.32	5.68
CaO	12.38	12.09	11.32	10.90	11.03	10.95	10.88	11.12	10.83
ZnO	b.d.l.	b.d.l.	b.d.l.	b.d.l.	b.d.l.	b.d.l.	b.d.l.	b.d.l.	0.15
Na_2O	2.19	2.36	1.58	1.96	2.10	2.13	2.24	2.47	2.11
K_2O	1.91	1.64	2.87	2.68	1.99	2.10	1.95	1.62	2.20
F	b.d.l.	b.d.l.	0.76	b.d.l.	b.d.l.	b.d.l.	b.d.l.	b.d.l.	b.d.l.
Cl	b.d.l.	0.03	0.06	b.d.l.	b.d.l.	b.d.l.	b.d.l.	b.d.l.	0.04
H_2O calc	2.02	2.00	1.54	1.92	1.96	1.96	1.97	1.98	1.91
Total	99.6	98.91	98.14	99.15	98.46	99.84	98.14	99.58	98.99
apfu									
Si	5.853	5.738	5.829	5.807	6.238	6.058	5.932	5.966	5.955
Al(4)	2.147	2.262	2.171	2.193	1.762	1.942	2.068	2.034	2.045
Σ T	8.000	8.000	8.000	8.000	8.000	8.000	8.000	8.000	8.000
Al(6)	0.510	0.397	0.429	0.425	0.420	0.409	0.447	0.418	0.446
Ti	0.214	0.301	0.210	0.229	0.011	0.268	0.322	0.357	0.200
Cr	0.000	0.006	0.000	0.004	0.004	0.004	0.006	0.000	0.001
Fe^{3+}	0.230	0.307	0.398	0.469	0.490	0.171	0.140	0.107	0.374
Mg	2.829	2.683	1.592	1.402	1.963	2.049	2.093	2.116	1.337
Zn	0.000	0.000	0.000	0.000	0.000	0.000	0.000	0.000	0.017
Fe^{2+}	1.209	1.296	2.247	2.333	1.933	2.100	1.992	2.002	2.461
Mn^{2+}	0.008	0.010	0.124	0.138	0.179	0.000	0.000	0.000	0.164
Σ C	5.000	5.000	5.000	5.000	5.000	5.001	5.000	5.000	5.000
Mn^{2+}	0.018	0.018	0.004	0.011	0.060	0.084	0.063	0.054	0.036
Ca	1.974	1.955	1.925	1.840	1.840	1.793	1.807	1.815	1.832
Na	0.008	0.028	0.072	0.149	0.100	0.109	0.114	0.125	0.132
Σ B	2.000	2.001	2.001	2.000	2.000	2.000	2.001	2.001	2.000
Ca	0.000	0.000	0.000	0.000	0.000	0.000	0.000	0.000	0.000
Na	0.624	0.663	0.415	0.450	0.534	0.522	0.559	0.605	0.513
K	0.363	0.316	0.581	0.539	0.395	0.410	0.386	0.315	0.443
Σ A	0.987	0.979	0.996	0.989	0.929	0.932	0.945	0.920	0.956
F	0.000	0.000	0.381	0.000	0.000	0.000	0.000	0.000	0.000
Cl	0.000	0.008	0.016	0.000	0.000	0.000	0.000	0.000	0.011
OH	2.000	1.992	1.602	2.000	2.000	2.000	2.000	2.000	1.989
Σ cation	15.987	15.98	15.997	15.989	15.929	15.933	15.946	15.921	15.956
#Mg	66.28	62.60	37.57	33.37	44.76	47.28	49.34	50.01	32.05
P (Mpa)						550 ± 138	700 ± 77	642 ± 71	
Species	pargasite	Ti-rich pargasite	potassic-ferro-pargasite	potassic-hastingsite	magnesio-hastingsite	ferro-pargasite	Ti-rich pargasite	Ti-rich pargasite	ferro-pargasite

References: Pgd: pegmatitic gabbroic dike; c: core; r: rim; a: aleatory; b.d.l.: below detection limit. Pressure calculations according to the Ridolfi et al. (2010) model. Formulae based on 23 atoms of oxygen equivalent, following the method of Hawthorne et al. (2012).

increase in Ti is analogous to the one observed by Brod et al. (2001) in micas from the Tapira complex and could be related to the combined effects of: (1) increasing oxygen fugacity and (2) Ti availability in the melt before the crystallization of titanian magnetite. The textural relationships between these phases in clinopyroxenite and mafic dikes show that biotite crystallizes earlier than interstitial titanian magnetite, thus the inflexion point in the curve of Fig. 7D could indicate an increasing consume rate of Ti in the melt due to oxide fractional crystallization and its impoverishment in more evolved rocks. The same Harker whole rock diagrams could be explained by the cumulate origin of some rocks.

The evolution of amphibole compositions is similar to the micas, with the Mg# decreasing from clinopyroxenite (66.28) to malignite, foid syenite and phonolite (33.37–32.05).

In phonolite dikes, some amphibole crystals show ovoid cores and finely zoned rims showing a marked compositional discontinuity, which suggests disequilibrium with compositional changes

Table 5
Representative compositions of trioctahedral micas from the La Peña complex.

Samples	LP D Bt 1	LP 12 Bt1	LP D Bt 2	LP B1 Bt 1	LP B1 Bt 2	LP 5c Bt 1	LP 5c Bt 2	LP 32D Bt 1	LP 32D Bt 2
Rock	Clinopyroxenite			Mafic dikes		Malignite		Tephritic dikes	
Analysis	86 a	16 r	91 a	1 a	3 c	7 r	9a	7 r	10 c
SiO_2 wt%	35.74	37.05	35.06	35.34	36.33	34.75	34.65	36.81	37.46
TiO_2	4.11	2.54	4.77	5.75	5.37	2.38	2.69	3.79	2.63
Al_2O_3	16.37	16.58	16.09	15.4	15.85	14.13	14.59	16.53	16.2
Cr_2O_3	b.d.l.	b.d.l.	0.05	b.d.l.	0.01	0.04	b.d.l.	0.01	0.02
FeO	13.19	10.18	15.21	16.77	14.3	23.59	22.4	11.99	10.88
MnO	0.18	0.28	0.15	0.37	0.35	0.73	0.76	0.1	0.12
MgO	15.53	18.65	13.78	11.99	14.22	10.66	10.49	16.9	18.57
CaO	b.d.l.	b.d.l.	b.d.l.	0.03	b.d.l.	b.d.l.	b.d.l.	0.07	0.39
BaO	0.29	0.15	1.59	b.d.l.	b.d.l.	b.d.l.	b.d.l.	b.d.l.	b.d.l.
Na_2O	0.23	0.15	0.28	0.3	0.24	0.31	0.31	0.38	0.39
K_2O	9.26	9.75	7.34	9.31	9.2	9.58	9.87	9.55	8.39
Cl	0.02	0.01	0.02	0.06	0.08	0.04	b.d.l.	0.02	0.02
F	b.d.l.	b.d.l.	b.d.l.	0.05	0.08	b.d.l.	b.d.l.	0.27	0.19
H_2O calc.	4.00	4.09	3.94	3.91	3.98	3.82	3.83	3.96	4.01
Total	98.92	99.43	98.27	99.25	99.96	100.02	99.59	100.26	99.18
apfu									
Si	5.342	5.426	5.328	5.360	5.388	5.432	5.416	5.384	5.474
Al(4)	2.658	2.574	2.672	2.640	2.612	2.568	2.584	2.616	2.526
ΣT	8.000	8.000	8.000	8.000	8.000	8.000	8.000	8.000	8.000
Al(6)	0.226	0.288	0.210	0.114	0.160	0.034	0.104	0.234	0.262
Ti	0.462	0.280	0.546	0.656	0.600	0.280	0.316	0.418	0.290
Cr	0.000	0.000	0.006	0.000	0.002	0.004	0.000	0.002	0.002
Fe	1.648	1.246	1.934	2.128	1.774	3.084	2.928	1.466	1.330
Mn	0.022	0.034	0.020	0.048	0.044	0.096	0.100	0.012	0.014
Mg	3.460	4.072	3.122	2.712	3.144	2.484	2.444	3.686	4.044
ΣO	5.820	5.922	5.836	5.656	5.722	5.982	5.892	5.818	5.944
Ca	0.000	0.000	0.000	0.004	0.000	0.000	0.000	0.010	0.062
Na	0.066	0.042	0.082	0.088	0.070	0.094	0.094	0.108	0.110
K	1.766	1.822	1.424	1.802	1.740	1.910	1.968	1.782	1.564
Ba	0.016	0.008	0.094	0.000	0.000	0.000	0.000	0.000	0.000
Σ	1.850	1.872	1.600	1.894	1.810	2.004	2.062	1.900	1.736
Cl	0.006	0.002	0.006	0.016	0.020	0.010	0.000	0.004	0.004
OH calc	3.994	3.998	3.994	3.960	3.942	3.990	4.000	3.870	3.908
F	0.000	0.000	0.000	0.024	0.038	0.000	0.000	0.124	0.088
Σ cation	15.670	15.794	15.436	15.552	15.532	15.988	15.954	15.718	15.678
Fe/(Fe + Mg)	0.32	0.23	0.38	0.44	0.36	0.55	0.55	0.28	0.25
Mg#	67.74	76.57	61.75	56.03	63.93	44.61	45.50	71.55	75.25

References: c: core; r: rim; a: aleatory. Formulae based on 24 atoms of oxygen equivalent. H_2O calculated as (2-F-Cl) (apfu).

in the melt (e.g.: high-pressure crystallization and low-pressure resorption or remixing with other melts).

In K-feldspars four different groups are observed (Fig. 8A and B). In groups 1, 2, and 3, Ba and Sr contents decrease with increasing K (*Or*). The slopes of trend lines decrease from malignite (1) towards foid syenite (2), reach a minimum in syenites and trachytic porphyries (4) and increase to phonolitic dikes (3). This behavior is ascribed to the depletion of Ba and Sr in the melt by fractional crystallization of plagioclase and K-feldspar. In foid syenites the K-feldspar shows similar Or values but lower Sr and Ba contents than microphenocrysts of the external unit of the malignite bodie (Fig. 8A and B). Both groups of K-feldspars define two different trends, suggesting that they belong to different batches of melt, which is in agreement with field observations. From the foid syenite to syenite and trachytic porphyries the contents of Sr in Kfs decrease suggesting extensive fractional crystallization of plagioclase prior to Kfs. In Kfs from the phonolite compositional variations linked to resorption episodes suggest periodic distabilization, possibly by different recharge events. These features plus the existence of mafic enclaves and the mingling relationships between tephrites and trachytes-phonolite strongly suggest that the LPC was an open magmatic system.

In nepheline, compositional variations show silica enrichment from malignite to foid syenite (Fig. 8C), in agreement with the evolution of nepheline from alkaline mafic magmas analyzed by Henderson and Gibb (1983), of tingüaites from Square Top studied by Wilkinson and Hensel (1994) and the ones from the Messum alkaline complex (Blancher et al., 2010). In all of these cases changes were interpreted as due to the differentiation of melts.

4.2. Whole rock geochemistry

The LPC has a wide compositional range (Table 10) with SiO_2 varying from 36.01 wt. % in clinopyroxenites to 58.84 wt. % in a syenite dike. Based on SiO_2 contents, rocks form three segments centered around 37, 45 and 55 wt.% that correspond to: 1) cumulate rocks (clinopyroxenite), 2) tephrite and malignite, 3) syenite, foid syenite, trachyte and phonolite. Between groups 1 and 2 there is a compositional gap due to the cumulate origin of clinopyroxenite. One particular feature of LPC rocks are the low MgO contents that

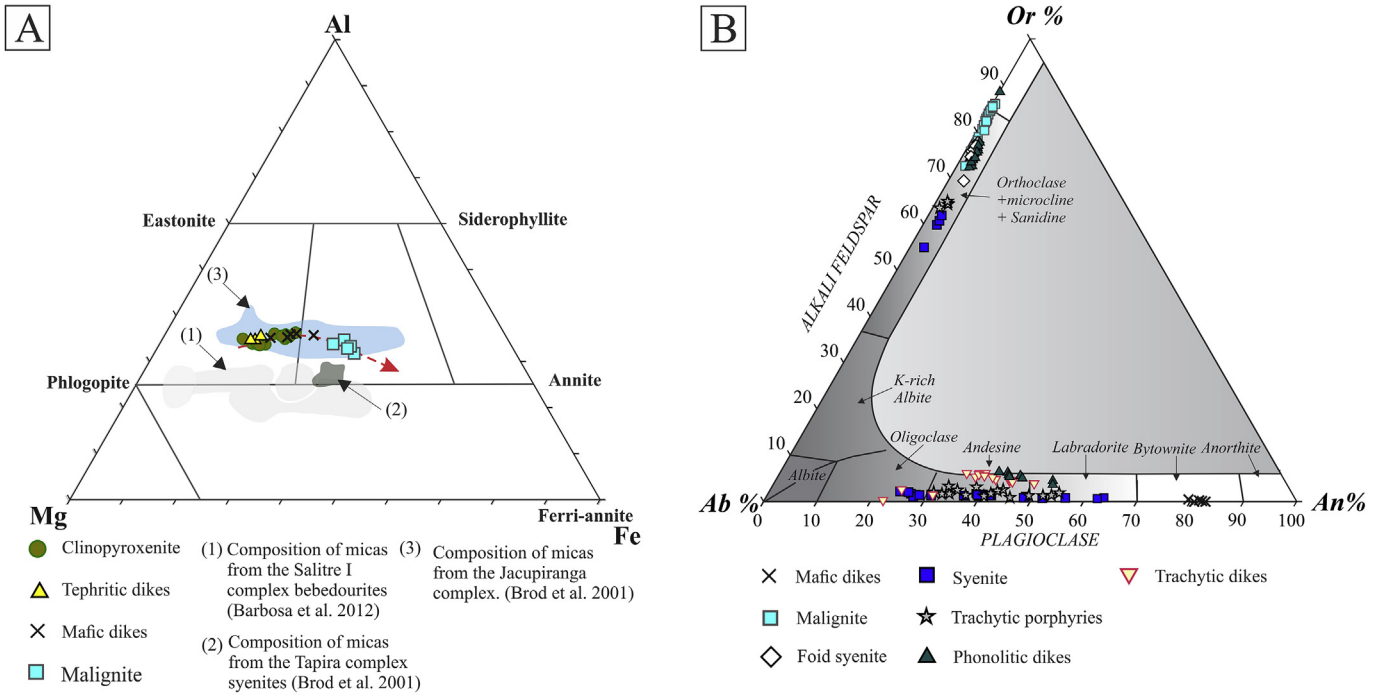

Fig. 5. A) Composition of the micas from the LPC in the Al-Fe_T-Mg triangular diagram in atoms per formula unit (*apfu*). The red line shows the evolution trend from clinopyroxenite to malignite; the fields 1, 2 and 3 correspond to micas from the Salitre I, Tapira and Jacupiranga complexes respectively. Note that the LPC micas are similar to the ones of the Jacupiranga alkaline complex. Diagram modified from Barbosa et al. (2012). B) Classification ternary diagram for feldspars from LPC.

Table 6
Representative compositions of feldspar from the La Peña complex.

Samples	LP 8 a Kfs	LP B1Pl	LP 62Kfs	LP 71 pl	LP 71 Kfs	LP 20 pl	LP 20 Kfs	LP D1 pl	LP D25 pl	LPD D25 Kfs
Rocks	Malignite	Mafic dikes	Foid syenite	Syenite		Trachytic porphyries		Trachytic dikes	Phonolitic dikes	
Analysis	2 c	4 c	1 c	9 a	18 r	1 c	13 c	6	4	24 r
SiO_2 wt. %	59.08	46.81	63.56	58.22	65.07	54.09	64.35	54.89	56.46	62.49
P_2O_5	b.d.l.	0.02	b.d.l.	b.d.l.	0.03	b.d.l.	b.d.l.	b.d.l.	0.01	b.d.l.
Al_2O_3	19.97	34.22	19.25	26.56	19.35	29.01	19.51	28.11	27.05	19.35
Fe_2O_3	0.09	0.59	0.09	0.13	0.17	0.24	0.21	0.36	0.26	0.02
MgO	b.d.l.	b.d.l.	b.d.l.	0.01	b.d.l.	b.d.l.	b.d.l.	b.d.l.	0.03	b.d.l.
CaO	0.21	16.26	0.22	7.41	0.51	10.72	0.50	9.82	7.85	0.01
SrO	2.23	0.74	0.51	0.03	0.08	0.53	0.31	0.24	1.39	0.46
BaO	3.86	0.03	0.43	b.d.l.	0.15	0.02	0.39	0.09	0.10	1.98
Na_2O	2.08	1.88	2.45	6.87	4.08	5.04	3.63	5.26	5.58	1.14
K_2O	10.73	0.06	12.21	0.22	9.88	0.24	10.81	0.56	1.20	13.49
Total	98.25	100.59	98.72	99.46	99.33	99.88	99.72	99.33	99.92	98.93
apfu										
Si	2.857	2.146	2.954	2.612	2.966	2.451	2.947	2.495	2.559	2.941
P	0.000	0.001	0.000	0.000	0.001	0.000	0.000	0.000	0.000	0.000
Al	1.138	1.849	1.055	1.404	1.040	1.549	1.053	1.506	1.445	1.073
Fe^{3+}	0.003	0.018	0.003	0.004	0.005	0.008	0.007	0.011	0.008	0.001
Mg	0.000	0.000	0.000	0.000	0.000	0.000	0.000	0.000	0.002	0.000
Ca	0.011	0.799	0.011	0.356	0.025	0.520	0.024	0.478	0.381	0.000
Sr	0.063	0.020	0.014	0.001	0.002	0.014	0.008	0.006	0.037	0.013
Ba	0.073	0.000	0.008	0.000	0.003	0.000	0.007	0.002	0.002	0.036
Na	0.195	0.167	0.220	0.597	0.361	0.443	0.322	0.464	0.491	0.104
K	0.662	0.004	0.724	0.013	0.574	0.014	0.632	0.032	0.069	0.810
Σcation	5.001	5.004	4.989	4.988	4.977	4.999	5.000	4.994	4.994	4.979
end member %										
Ab	22.47	17.21	23.07	61.81	37.60	45.32	32.95	47.60	52.14	11.38
An	1.23	82.41	1.14	36.89	2.57	53.26	2.50	49.07	40.50	0.03
Or	76.30	0.38	75.79	1.30	59.83	1.52	64.55	3.33	7.36	88.59

References: c: core; r: rim; a: aleatory. Formulae based on 8 atoms of oxygen.

Table 7
Representative compositions of nepheline from the La Peña complex.

Samples	LP 8a Ne 1	LP 8a Ne 1	LP 62 Ne1	LP 62 Ne1
Rocks	Malignite		Foid syenite	
Analysis	26 c	27 c	1 c	2 r
SiO_2 wt. %	43.29	42.95	43.23	43.14
Al_2O_3	33.27	33.36	34.45	34.14
Fe_2O_3	0.46	0.44	0.34	0.38
CaO	1.34	1.34	2.36	2.48
Na_2O	15.89	15.87	14.71	14.61
K_2O	5.27	5.25	4.68	4.49
Total	99.51	99.20	99.77	99.24
Si	8.339	8.303	8.258	8.278
Al	7.554	7.600	7.756	7.723
Fe^{3+}	0.067	0.064	0.049	0.055
ΣT	15.960	15.967	16.063	16.056
Ca	0.276	0.277	0.483	0.509
Na	5.934	5.948	5.447	5.434
K	1.295	1.293	1.141	1.099
Σ (A + B)	7.505	7.519	7.071	7.043
Σcation	23.465	23.486	23.134	23.099
end member %				
Ne	74.99	75.04	71.11	71.02
Ks	18.20	18.14	16.56	15.97
An	6.81	6.82	12.33	13.01
Ne	77.98	78.27	77.68	78.05
Ks	18.92	18.92	18.09	17.55
Qtz	3.10	2.82	4.24	4.40

References: c: core; r: rim. Formulae based on 32 atoms of oxygen.

Table 8
Representative compositions of apatite from the La Peña complex.

Samples	LP 12 Ap 1	LP B1 Ap 2	LP 5 Ap1	LP 32D Ap 3
Rocks	Clinopyroxenite	Mafic dikes	Malignite	Tephritic dikes
Analysis	114 c	4 r	39 n	9 a
P_2O_5	40.06	40.7	39.46	40.12
SiO_2	0.76	0.65	1.00	1.42
FeO	0.17	0.23	0.00	0.17
MnO	0.01	0.06	0.00	0.02
CaO	53.73	53.95	54.00	54.36
SrO	0.05	0.32	0.80	0.15
Na_2O	0.01	0.02	0.00	0.05
La_2O_3	–	0.15	0.20	b.d.l.
Ce_2O_3	–	0.44	0.53	0.19
Nd_2O_3	–	0.51	0.30	b.d.l.
SO_3	0.91	0.50	0.44	1.08
F	2.35	2.39	3.27	1.43
Cl	0.41	0.26	0.00	0.18
H_2O calc	0.52	0.56	0.243	1.04
Total[a]	97.90	99.67	99.77	99.57
apfu				
P	2.929	2.937	2.885	2.884
Si	0.066	0.055	0.086	0.121
Fe^{2+}	0.012	0.016	0.000	0.012
Mn	0.001	0.004	0.000	0.001
Ca	4.972	4.927	4.997	4.946
Sr	0.003	0.016	0.040	0.007
Na	0.002	0.003	0.000	0.008
La		0.005	0.006	0.000
Ce		0.014	0.017	0.006
Nd		0.016	0.009	0.000
S	0.059	0.032	0.028	0.069
F	0.642	0.644	0.893	0.384
Cl	0.060	0.038	0.000	0.026
OH calc	0.298	0.318	0.185	0.590
Σ cation	4.989	5.000	5.069	4.981
P + Si + S	3.053	3.024	3.000	3.074

[a] Includes correction for F≡O and Cl≡O. References: c: core; r: rim; a: aleatory. -: not measured b.d.l.: below detection limit. Yttrium sought but not detected. H_2O calculated as (1-F-Cl) (apfu).

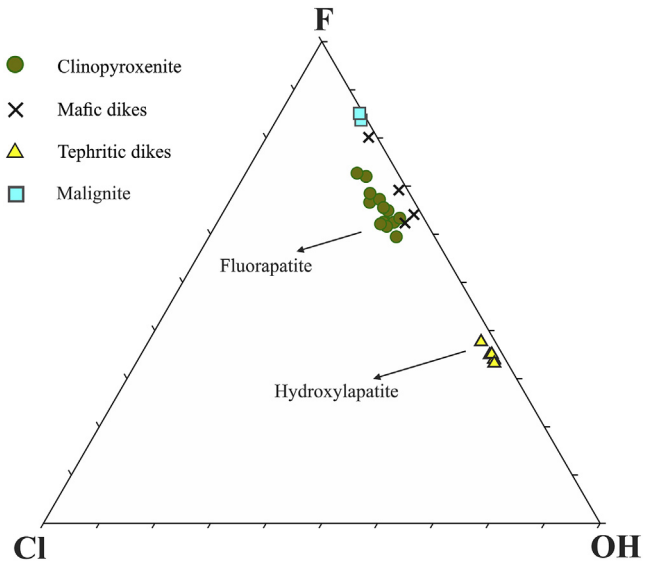

Fig. 6. Ternary diagram for monovalent anions in apatite from LPC. Two groups are distinguished: hydroxylapatite in the tephrites and fluorapatite in the other rocks.

Table 9
Representative compositions of garnet from the La Peña complex.

Samples	LP 5c Grt 1	LP 8a Grt 1	LP D25 Grt 1	LP D25 Grt 1
Rocks	Malignite		Phonolitic dikes	
Analysis	16a	68 c	1 r	2 r
SiO_2 wt. %	36.84	33.72	35.01	35.17
TiO_2	3.10	6.22	3.51	3.26
ZrO_2	0.08	–	0.20	0.24
Al_2O_3	4.74	5.87	6.95	7.14
V_2O_3	0.28	–	0.18	0.30
Cr_2O_3	0.02	0.03	b.d.l.	b.d.l.
Fe_2O_3	18.23	18.51	18.45	18.40
FeO	4.70	1.70	2.61	2.75
MnO	0.68	1.11	1.31	1.29
MgO	0.25	0.45	0.33	0.21
CaO	31.70	32.90	31.69	32.02
P_2O_5	0.02	–	0.08	0.17
Na_2O	0.10	0.03	0.04	b.d.l.
Total	100.74	100.55	100.35	100.94
apfu				
Si	3.013	2.763	2.862	2.859
Ti	0.190	0.383	0.216	0.199
Zr	0.003		0.008	0.009
Al	0.456	0.567	0.670	0.684
V	0.018		0.012	0.019
Cr	0.002	0.002	0.000	0.000
Fe^{3+}	1.122	1.142	1.135	1.126
Fe^{2+}	0.321	0.117	0.179	0.187
Mn	0.047	0.077	0.090	0.089
Mg	0.031	0.055	0.040	0.026
Ca	2.778	2.889	2.776	2.790
P	0.002		0.006	0.012
Y	0.000	0.000	0.000	0.000
Na	0.016	0.004	0.006	0.000
end member %				
Py	0.97	1.76	1.31	0.83
Alm	10.06	3.71	5.78	6.04
Sp	1.47	2.46	2.93	2.88
And	62.62	61.47	59.49	58.98
Gro	24.38	30.46	30.30	31.28

References: c: core; r: rim; a: aleatory. . -: not measured b.d.l.: below detection limit. Yttrium sought but not detected. Formulae based on 12 atoms of oxygen and 8 cations, following Droop (1987).

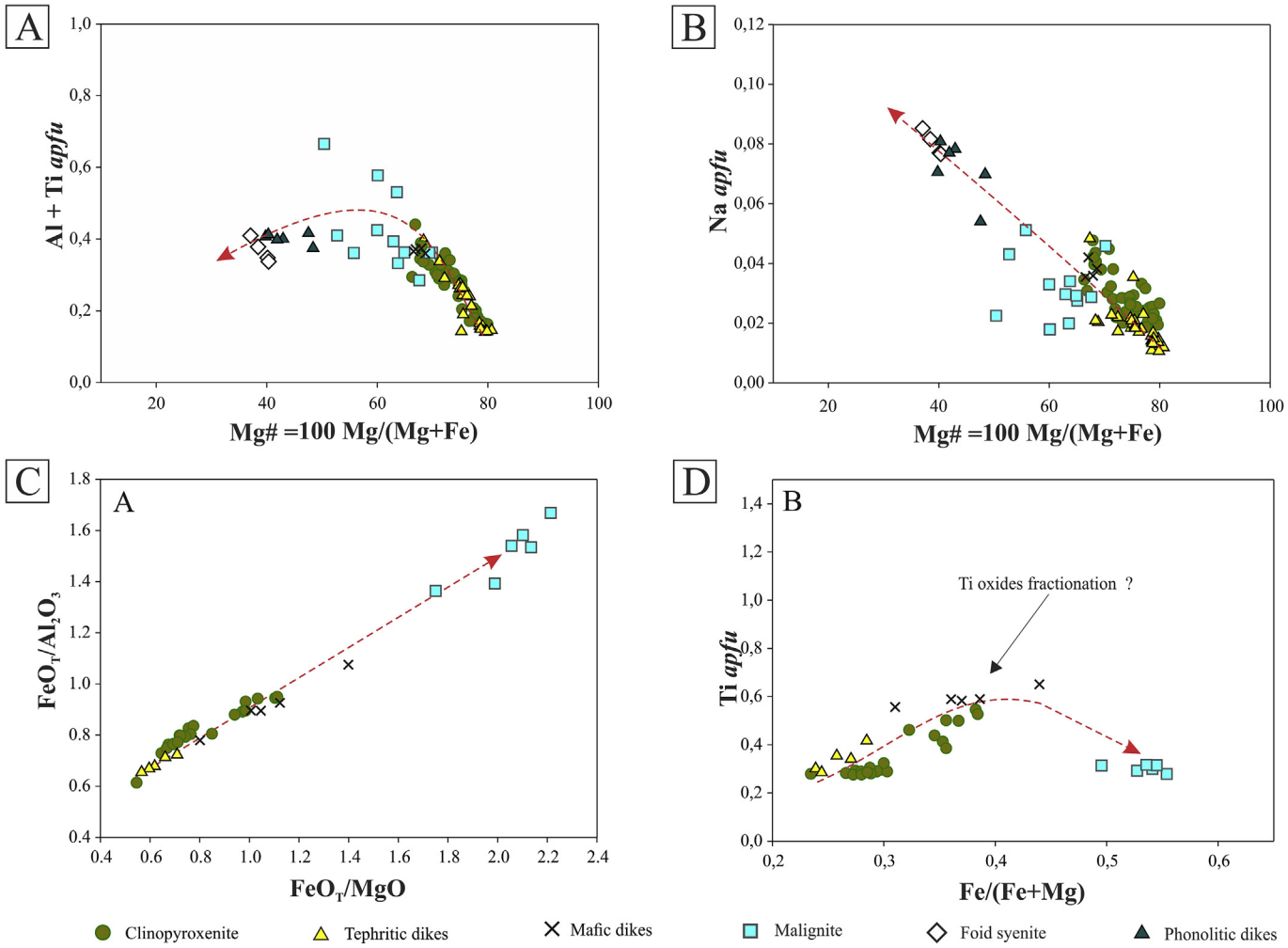

Fig. 7. A) and B) Variation diagrams showing the compositions of the clinopyroxene from LPC. C) and D) Variation diagrams showing the mica compositions of the LPC. The evolution trends are highlighted by the dashed red line. In D) is indicated the possible starting point of Ti-oxide fractionation.

range from 4.45% in tephritic dikes to 0.51% in foid syenite. In contrast, the content in cumulate rocks is higher, from 8.73 to 9.30 wt.%, but they do not represent melt compositions. Excluding cumulate rocks, Mg# varies from 39 to 36 in rocks of group 2, and from 30 to 21 in rocks of group 3. In the TAS classification (Le Bas et al., 1986) the LPC rocks plot in the field of the alkaline series, mostly in the subfield of mid alkalinity (Fig. 9). The alkalis ($K_2O + Na_2O$, in wt.%) vary from 0.90 to 1.09 in rocks from group 1, from 6.01 to 8.30% in group 2, and from 9.61 to 12.13% in group 3. The K_2O/Na_2O ratios vary from 1.15 to 1.95, thus classifying the rocks as belonging to the potassic series, except for syenite and trachyte that are slightly sodic. Using the criteria of Foley et al. (1987) none of the analyzed rocks in this paper is ultrapotassic ($K_2O > 3\%$; $K_2O/Na_2O > 2$ for $MgO > 3\%$).

As shown by Harker diagrams of the LPC rocks (Fig. 10), the increase of SiO_2 from group 1 to 3 is associated to decreasing MgO, CaO, Fe_2O_3, TiO_2 and P_2O_5 and increasing Al_2O_3, K_2O and Na_2O. Trends are consistent with the observed petrographic features and the variation of mineral chemical composition with differentiation of melts. Cr (<20 ppm) and Ni (<30 ppm) have low contents. The trace elements pattern normalized to OIB values show a relatively flat design, with LILE and Pb enrichment and HFSE (plus P and Ti for the rocks of group 3) depletion (Fig. 11A).

The enrichment in incompatible elements is also seen in MORB-normalized patterns (Fig. 11B), coupled with negative anomalies in Nb and Ta with respect to Th and Ce. Covariant La/Nb vs La/Ba diagrams (Fig. 11C) show that the LPC rocks plot close to arc basalts, whereas in the Th/Yb vs Ta/Yb diagram (Fig. 11D) they plot in the field of basalts from Central Andes. The REE patterns (Fig. 12A) show no Eu anomaly and a smooth negative slope, with La/Yb_N in the range of 11–14.4, Dy/Lu_N between 1.05 and 1.9, and high Lu_N contents (9.6–16.6).

5. Discussion

5.1. The source of the LPC magmas

Based on the flat trace element content normalized to OIB, Villar and Zappettini (2000) interpreted that the primary magma was derived from the mantle and had a composition close to malignite. Based on this and the Pb isotopic data, Lucassen et al. (2007) suggested that LPC melts derived from a depleted lithospheric mantle contaminated with small quantities of a different crustal material. Zappettini et al. (2013), based on new geochemical and isotopic data (Sr, Nd, Pb), suggested an asthenospheric source and the mixing between this depleted source with an enriched lithospheric

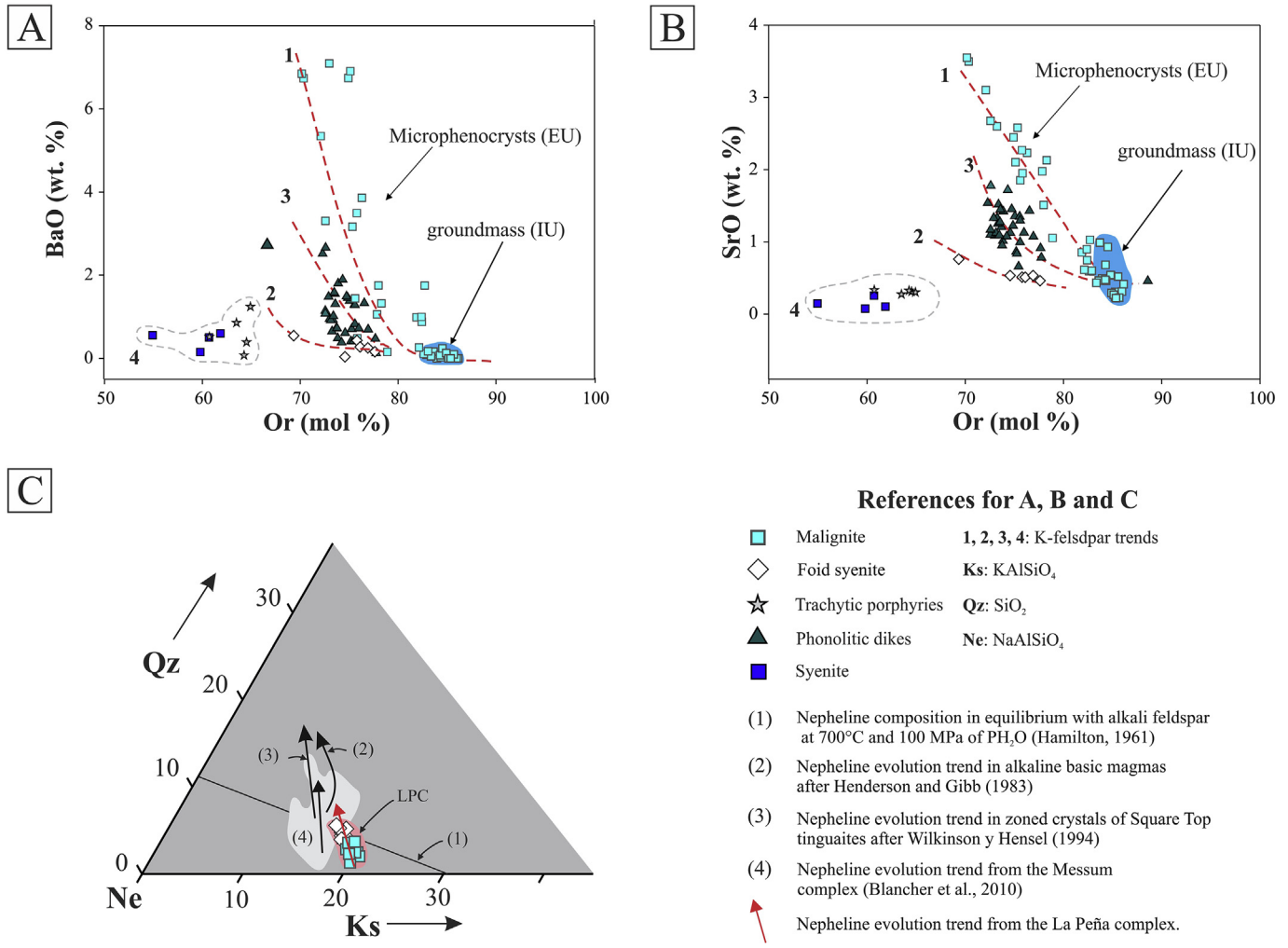

Fig. 8. A) and B) Variation diagram of minor and trace elements in K-feldspar from LPC, with indication of trends 1, 2, and 3. C) Ternary diagram Ks (Kalsilite) - Qz (Quartz) - Ne (Nepheline) showing the composition of nepheline from the LPC compared with other alkaline complex, and with nepheline compositions in equilibrium with alkali feldspar at 700° and 100 MPa of PH_2O (Hamilton, 1961). Arrows show the different evolution trends.

component derived from delaminated lower crust. They proposed a model via partial melting of a metasomatized garnet-rich mantle with phlogopite, carbonates and variable quantities of a spinel mantle.

The chemical analyses performed in this work show that these rocks have a pattern of trace elements similar to arc basalts and other arc manifestations of Miocene age (Fig. 11A and B). Moreover, in terms of typical trace element ratio diagrams (Fig. 11C and D) the LPC rocks plot in the field of Pleistocene-Holocene arc basalts and in the Central Andes basalts. Additionally, extended trace element diagrams (e.g., Fig. 11B) clearly shows enrichment in incompatible elements (Sr, K, Rb, Ba, Th) and negative anomalies in Nb and Ta respect to Th and Ce generally interpreted as typical of subduction related volcanic arc rocks (Pearce, 1982, 1996; Baier et al., 2008). Most of the analyzed rocks of LPC have La/Ta ratios similar to Andean volcanic rocks (Hickey et al., 1986). The Pb enrichment compared to Ce (Fig. 11A) also suggests a possible Pb input from subduction-derived fluids. In contrast, Zappettini et al. (2013), based on the Th/U enrichment, consider that there is a lack of subduction-related components in the LPC. However, we consider that the same result could be obtained by contamination with a granulitic lower crust, whose composition always shows increased Th/U ratios (Rudnick and Fountain, 1995). The evidences suggest a strong subduction signal in the magmas of LPC.

The mildly high $(La/Yb)_N$ ratios, the smooth slope in heavy REE pattern (Fig. 12A) and the low Lu_N contents of the LPC also suggest that garnet did not participate in melting reactions in the source, at least in significant amounts.

Miller et al. (1999), in their study of the ultrapotassic lavas of SW Tibet, suggested that the high K/Nb (1241–2278) and low U/Pb (0.2–0.5) ratios associated with high Rb/Sr relationships could be possible if phlogopite participates in the melting reactions. The same interpretation is applicable to LPC that shows high K/Nb (2213–3822) and low U/Pb (0.03–0.35) values.

Taking these data into account, the primary magma of LPC most probably originated in a lithospheric depleted mantle (as stated also by Lucassen et al., 2007), formed mainly by spinel lehrzolites (with some possible participation of minor garnet), in presence of phlogopite generated by metasomatism linked to subduction derived fluids.

Zappettini et al. (2013) indicated that a local asthenospheric mantle upwelling could have initiated the heat advection that triggered the potassic magmatism, whose location and ascent would have been related to a local lithospheric thinning originating

Table 10
Whole rock compositions of rocks representative from the LPC.

Samples	LP 12a	LP 12c	LP 12d	LP 6	LP D32	LP 62	LP 71	LP D17	LP D1	LP 97	LP D25
Rocks	Clinopyroxenite			Malignite	Tephrite[a]	Foid syenite	Syenite		Trachyte[b]		Phonolite[c]
Group	1			2		3					
SiO_2 (wt. %)	37.33	36.01	38.20	45.98	43.03	52.48	56.92	58.84	57.44	54.90	50.41
TiO_2	2.19	2.45	2.15	1.50	1.63	0.46	0.86	0.57	0.60	0.61	0.64
Al_2O_3	5.84	6.05	6.07	14.75	12.95	21.34	18.44	19.37	17.97	17.71	20.38
Fe_2O_3	21.57	24.39	20.54	11.66	13.64	3.79	5.99	3.79	5.18	5.28	4.80
MnO	0.27	0.33	0.26	0.24	0.24	0.15	0.18	0.17	0.11	0.17	0.24
MgO	9.22	8.73	9.30	3.32	4.45	0.51	1.29	0.55	0.77	0.90	0.83
CaO	19.81	19.64	21.07	10.88	12.15	5.69	5.56	4.64	4.01	5.68	6.54
Na_2O	0.40	0.29	0.36	2.82	2.05	3.92	5.08	5.12	5.23	4.71	5.65
K_2O	0.69	0.63	0.54	5.48	3.96	7.65	4.53	4.97	5.04	6.12	6.48
P_2O_5	1.96	1.76	2.11	0.83	1.34	0.11	0.26	0.10	0.19	0.17	0.12
LOI	0.23	0.32	0.25	0.94	3.96	3.27	0.53	0.75	1.34	1.87	4.69
Total	99.3	100.3	100.6	97.5	95.4	96.1	99.1	98.1	96.5	96.3	96.1
Sc (ppm)	88.0	88.0	86.0	26.0	35.0	3.0	6.0	2.0	5.0	5.0	2.0
Be	1.0	<1	<1	4.0	3.0	4.0	3.0	3.0	5.0	5.0	8.0
Ba	230.0	62.0	199.0	952.0	692.0	1304.0	983.0	1553.0	1383.0	876.0	903.0
Rb	21.0	28.0	19.0	100.0	80.0	155.0	108.0	102.0	101.0	182.0	133.0
Sr	510.0	506.0	551.0	1536.0	1590.0	3622.0	1379.0	1867.0	1167.0	1399.0	3038.0
Zr	107.0	90.0	120.0	208.0	127.0	133.0	275.0	166.0	311.0	258.0	279.0
Nb	2.5	1.7	1.8	11.9	8.7	12.6	14.2	18.4	15.1	19.1	24.3
Ni	<20	<20	30.0	<20	<20	<20	<20	<20	<20	<20	<20
Co	68.0	72.0	74.0	28.0	39.0	6.0	7.0	4.0	5.0	8.0	5.0
Zn	140.0	200.0	140.0	120.0	150.0	60.0	120.0	70.0	60.0	310.0	90.0
Cr	<20	<20	<20	<20	<20	<20	<20	<20	<20	<20	<20
Y	26.4	20.6	25.8	28.8	25.1	19.1	30.5	29.0	25.7	23.8	40.1
Cs	1.1	2.1	1.0	1.9	0.7	2.8	3.9	2.4	1.3	7.9	3.8
Ta	0.2	0.1	0.1	0.6	0.6	0.6	0.7	1.0	0.6	0.9	1.0
Hf	3.8	3.4	4.1	5.0	3.4	2.9	6.4	3.9	6.7	5.3	5.8
Th	1.9	1.2	1.4	4.0	4.4	5.0	5.9	4.1	7.6	12.1	11.5
U	0.5	0.4	0.4	1.5	1.5	1.9	2.2	1.3	2.8	4.0	5.3
V	643.0	782.0	625.0	368.0	459.0	114.0	108.0	57.0	101.0	114.0	126.0
Cu	1170.0	450.0	1320.0	210.0	460.0	70.0	10.0	20.0	<10	40.0	50.0
Ga	17.0	19.0	17.0	22.0	20.0	19.0	22.0	19.0	22.0	23.0	25.0
Ge	2.8	2.8	2.8	2.1	2.5	1.5	1.9	2.0	1.9	1.9	2.2
Pb	9.0	<5	6.0	14.0	39.0	14.0	18.0	13.0	17.0	62.0	15.0
La	28.5	21.4	27.3	33.2	32.5	35.6	47.2	42.6	47.9	58.6	76.4
Ce	70.3	53.5	66.8	79.8	73.4	74.5	96.6	95.4	91.1	113.0	149.0
Pr	9.9	7.7	9.4	10.9	9.4	9.0	11.5	12.1	10.3	12.4	17.1
Nd	48.7	38.1	47.1	48.6	41.8	35.5	47.6	50.9	39.3	45.0	67.4
Sm	11.0	9.3	11.1	10.9	9.1	6.5	9.3	9.5	7.4	7.6	13.3
Eu	3.3	2.8	3.5	3.3	2.7	2.0	2.7	3.1	2.1	1.9	4.0
Gd	9.8	8.1	9.8	9.2	7.9	5.3	7.7	7.9	6.1	5.9	10.9
Tb	1.3	1.0	1.2	1.3	1.0	0.7	1.1	1.1	0.8	0.8	1.5
Dy	5.7	4.6	5.6	6.2	5.0	3.5	5.6	5.4	4.2	3.9	7.6
Ho	1.0	0.7	0.9	1.1	0.9	0.7	1.1	1.0	0.8	0.8	1.4
Er	2.4	1.9	2.3	2.7	2.3	1.8	3.1	2.8	2.4	2.3	4.0
Tm	0.3	0.2	0.3	0.3	0.3	0.3	0.5	0.4	0.4	0.3	0.6
Yb	1.8	1.4	1.7	2.0	2.0	1.7	3.1	2.4	2.5	2.2	3.6
Lu	0.3	0.2	0.3	0.3	0.3	0.2	0.5	0.4	0.4	0.4	0.5
#Mg				36	39	21	30	22	23	25	26
K_2O/Na_2O				1.94	1.93	1.95	0.89	0.97	0.96	1.30	1.15

[a] Tephritic dikes
[b] Trachytic dike (LPD1) and trachytic porphyry (LP97)
[c] Phonolitic dike. LPD32, LP6, LP12c, LP12a samples were used in the mass-balance fractionation model.

by extension in this back-arc position. However, the arc signature of LPC rocks suggest slab fluids were involved in the generation of these magmas. Possibly, subduction-derived fluids interacted with the asthenosphere reaching the lithospheric mantle; a local adiabatic decompression of modified asthenosphere (through metasomatism caused by fluids liberated from the subducted plate) caused melting of the astenosphere wedge, which acted only as a heat source for the melting of the overlying lithospheric mantle (also modified). These conditions could be linked to the combination of subduction, and a transtensional regime in the back-arc area (see Pagano et al., 2014).

5.2. The nature of the initial magma and its evolution

Villar and Zappettini (2000) and Zappettini et al. (2013) suggested that the initial magma of the LPC had composition close to the malignite. In the latter paper they showed the isotopic link between malignite and clinopyroxenite and considered the first as the initial magma in equilibrium with the second. This interpretation considers the malignite as the parental magma that originated the clinopyroxenite by sedimentation and the syenite and related rocks as produced by fractional crystallization. Alternatively, Pagano et al. (2014) considered that the parental magma had a

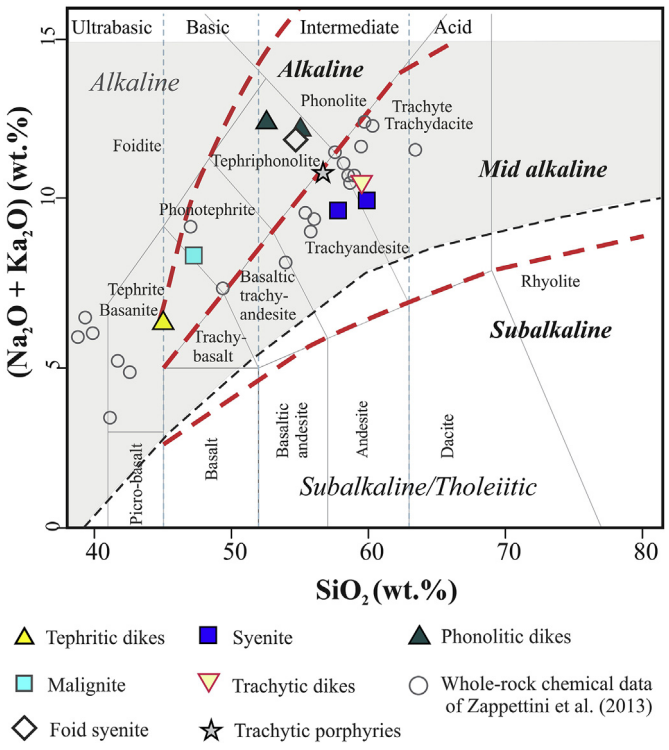

Fig. 9. TAS classification diagram (Le Bas et al., 1986) for volcanic rocks. The dashed black lines divide the sub- and alkaline fields after Irvine and Baragar (1971). The dashed red lines correspond to the isoplets sigma after Rittmann (1957) which define the subalkaline, medium alkaline and alkaline magmatic lineage.

composition close to basanite, represented by the late basanitic dikes, now reclassified as tephritic dikes (with <10% of normative olivine). The supporting evidences are: (1) tephritic dikes are higher in MgO and poorer in SiO_2 and alkalis than the malignite, (2) clinopyroxene and biotite from tephrites are less evolved than the ones from malignite, and (3) a good correlation exists between the chemical composition of the clinopyroxene from clinopyroxenite and tephrites; the same situation is observed for phlogopite (Fig. 7). As clinopyroxene from tephritic dikes shows equilibrium with the melt, it is interpreted that clinopyroxene of the cumulate clinopyroxenite had been in equilibrium with a compositionally similar melt; i.e. similar to tephritic dikes. Mass balance calculations of fractional crystallization of basanitic parental magmas (Morbidelli et al., 1995) show that the extensive fractional crystallization of mafic minerals (olivine and pyroxene) should drive the residual low-temperature melts toward syenitic (trachytic) or phonolitic compositions. In the LPC the evolution from basanites-tephrites to syenitic melts is reasonable, as suggested by results of mass balance calculations (Table 11). This result shows that fractional crystallization of 19% of an assemblage composed of 70% clinopyroxene, 23% magnetite and 7% apatite (modally similar to clinopyroxenite), and considering the malignite as a residual evolved melt, a theoretical parental magma of tephritic composition is obtained. Thus we considered that the parental tephritic magma fractionated the clinopyroxenite, leaving as remnant a relatively evolved syenitic melt that crystallized as malignite. Additional support is found in the similar Sr isotope content that suggests equilibrium between the two rocks (data from Lucassen et al., 2007; Zappettini et al., 2013) hereafter considered as cumulate and residual evolved melt respectively. It should be noted that tephritic dikes are considered compositionally equivalent to the parental magma, but emplaced at a late stage. Mafic dikes that intruded the cumulate clinopyroxenite, are interpreted as slightly more evolved intercumulus melts, based on the *in situ* occurrence and structural arrangement and on the comparatively more evolved chemical composition of clinopyroxene and biotite (Fig. 7).

The variation diagrams of LPC rocks show an evolution trend from rocks of group 2 (tephrite-malignite) to group 3 (syenite-trachyte-phonolite) defined by decreasing contents of Fe, Ti, P, Ca and Mg (and K to a lesser degree), and increasing contents of Si, Al and Na. In the same way, nepheline composition shows a differentiation trend from malignite to syenite. However, the field relationships clearly show that rocks of group 3 are emplaced as late batches, suggesting deeper fractionation of these melts. Pagano et al. (2014), based on detailed structural analyses and field relationships, suggested that LPC formed by juxtaposition of different batches of melts fractionated in a deep reservoir and emplaced at shallow levels. The geobarometer approach, applying the model of Ridolfi et al. (2010) to amphibole phenocrysts hosted in a trachyte dike, gives equilibrium pressures between 550 ± 138 MPa (~20.7 km) and 700 ± 77 MPa (~26.5 km) (Table 4), which to our view could approximately indicate the depth of this magmatic reservoir. Zappettini et al. (2013), based on the Ridolfi and Renzulli (2012) amphibole geobarometer applied to malignite, considered that all rocks from LPC are derived from a common parental magma localized in a reservoir at approximately 30 km depth.

The geodynamic setting in the region at 19 Ma, characterized by a strong compressive stage (Kay and Mpodozis, 2002), would be appropriate for precluding the fast ascent of magma trough the crust, allowing its residence in intracrustal magmatic chambers as suggested by some authors (e.g., Richards et al., 2001; Maydagán et al., 2011). The opening of extensional NNW-SSE fractures linked to a local strike-slip brittle shear zone would have allowed the ascent of successive batches of melt up to the present emplacement of the LPC at shallow levels (Pagano et al., 2014). Based on geological criteria we estimate this depth in less than 5 km; the evidences are: 1) straight and sharp contacts between different units, 2) presence of an extensive breccia zone and abundant dikes, suggesting a very fragile behavior of the rocks, 3) subhorizontal dikes indicating low pressure of confinement, 4) host rocks (Villavicencio Fm) with very low regional metamorphic degree, 5) presence of a contact aureole with cordierite (Zappettini et al., 2013) and 6) porphyritic and microporphyritic textures, which suggest a strong thermal contrast with the country rock.

The low Mg# and Cr and Ni contents of all the LPC rocks show that they derive from magmas that are: a) not directly mantle-derived, and b) have undergone significant high-pressure differentiation before. The most plausible explanation is that early crystallization of olivine, Cr-rich pyroxene and Cr-rich spinel in a deep magma chamber system depleted a primary mantle-derived basanitic melt of these components leaving a slightly more evolved tephritic magma. The results also show that Mg and Ca in the LPC rocks are concentrated in the cumulate (clinopyroxenite) and progressively decrease towards evolved terms controlled by the fractionation of calcic clinopyroxene (diopside-hedenbergite). In the same way, the positive correlation of MgO vs CaO/Al_2O_3 and MgO vs Sc/Y (Fig. 12B) suggest the continuous and decreasing fractionation of clinopyroxene (Mattsson and Oskarsson, 2005). The decrease of Ti and Fe with SiO_2 increment (Fig. 10) evidences the abundant crystallization of Fe–Ti oxides in rocks of group 1, and this trend decreases towards the most differentiated rocks. Decreasing P contents are controlled by continuous fractionation of apatite. Al, K and Na are controlled by feldspar fractionation in evolved rocks (Fig. 10). In this case, the transition from syenite (trachyte) to phonolite can be explained by the plagioclase effect (Bowen, 1945) assisted by the orthoclase effect (Bailey and Schairer,

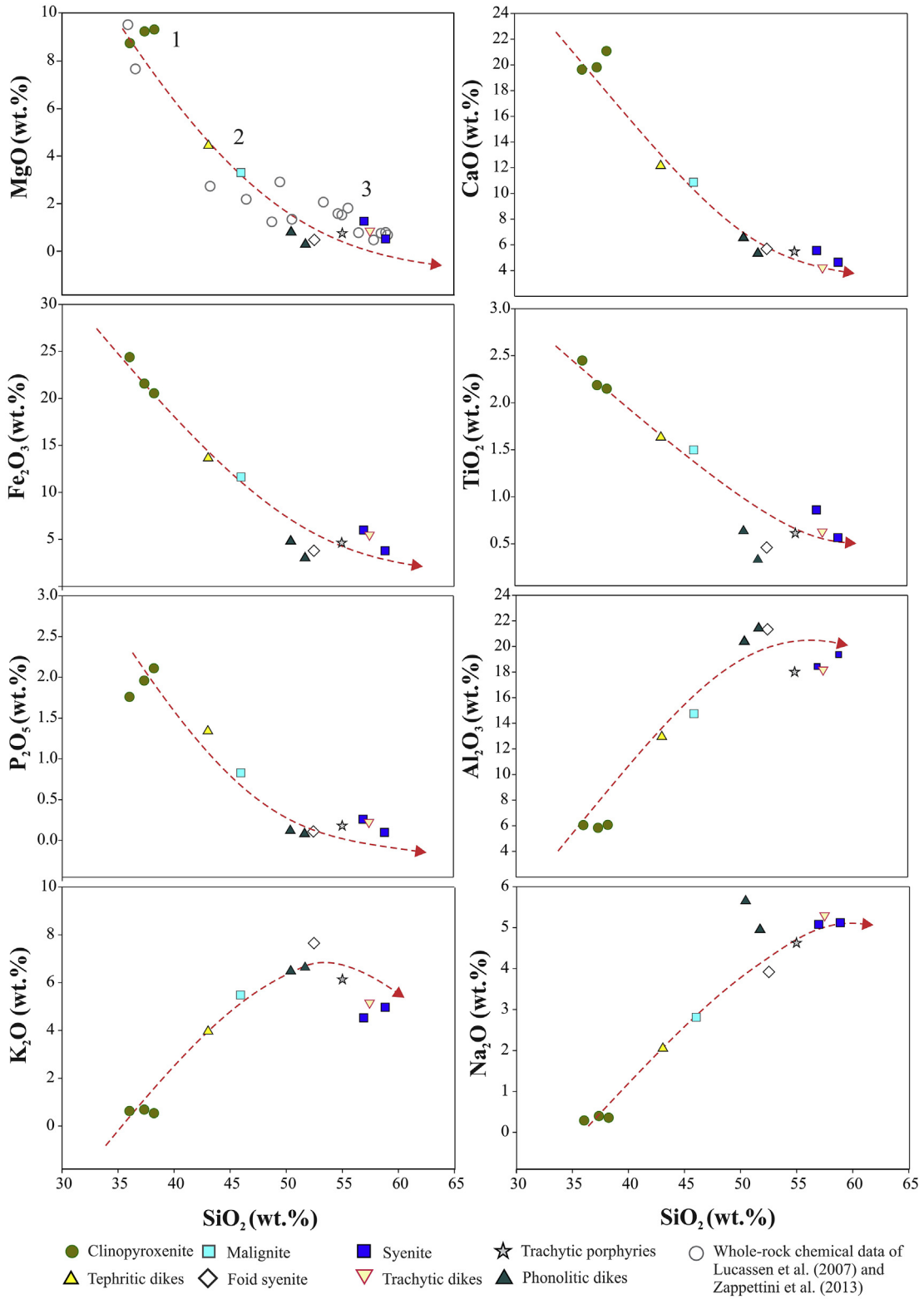

Fig. 10. Harker variation diagrams showing the compositions of the LPC rocks. Dashed red lines show the evolution trends. The empty gray circles correspond to data from Lucassen et al. (2007) and Zappettini et al. (2013).

1964). The uptake of Ca and Al by plagioclase led to a Na- and K-enriched melt; precipitation of K-feldspar led to further Na increase, stabilizing sodalite in the final stages of crystallization of the phonolitic dikes. The compositional variations linked to resorption surface observed in Kfs from phonolitic dikes, in addition to the existence of mafic enclaves and the mingling relationships between tephrite-basanite and trachyte-phonolite, suggest recharge events with local mixing at least at the last stages of LPC evolution. The

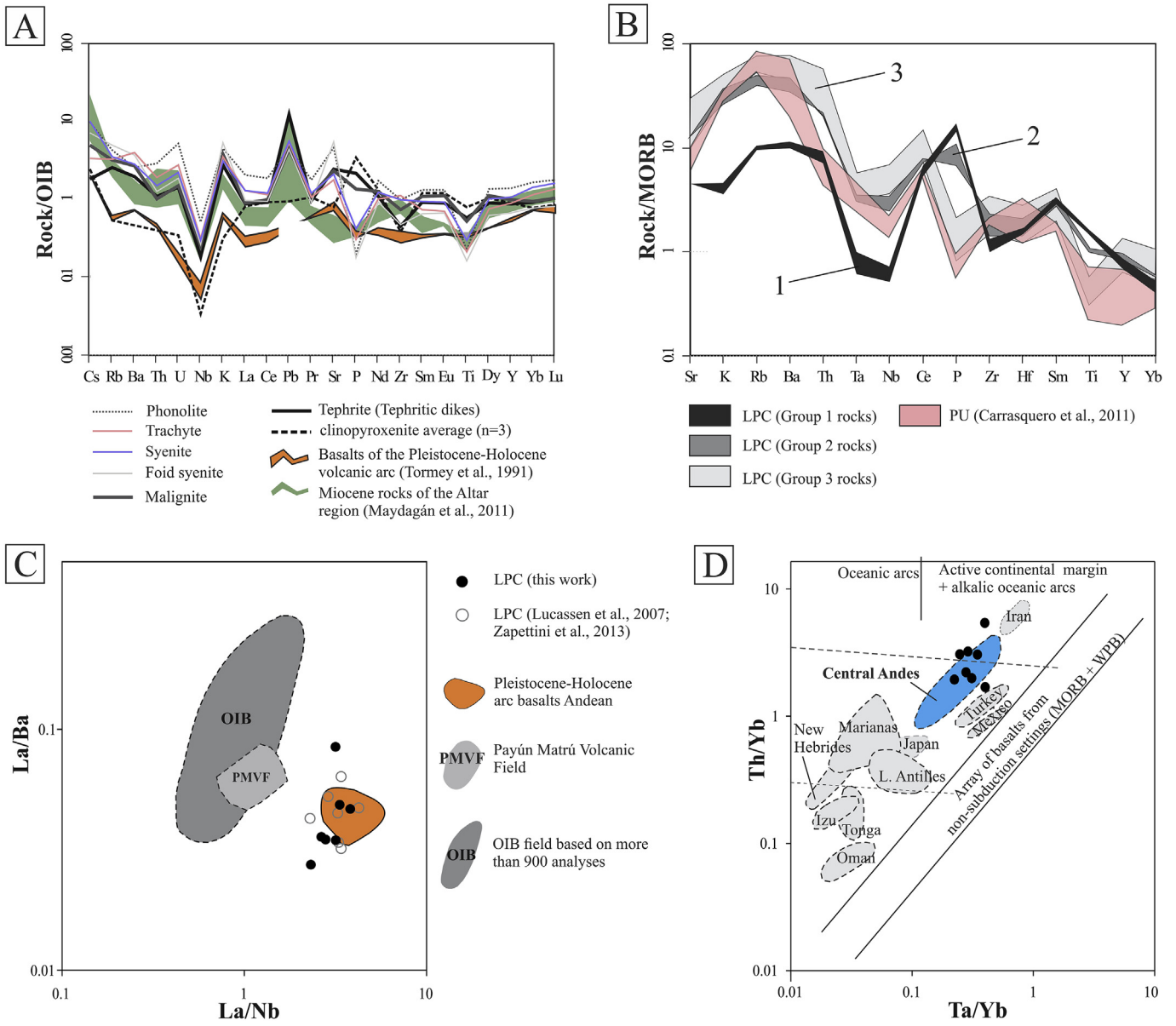

Fig. 11. A) Spider trace element diagram normalized to ocean island basalts (OIB) (Sun and McDonough, 1989) showing the different rocks of the LPC compared with the arc basalt compositions after Tormey et al. (1991) and the arc Miocene rocks of the Altar region after Maydagán et al. (2011). Note the strong Pb positive anomaly and the negative ones for Nb and Ti. B) Trace elements diagram of rocks from LPC compared with rocks from Paramillos de Uspallata (PU), normalized to MORB (Pearce, 1983). Note the similarity of the patterns; the most striking difference is in the higher P content of the LPC rocks (group 1 and 2). Note the LILE (Sr, K, Rb, Ba) and Th enrichment and the negative anomalies for Nb, Ta, and Ti. C) Covariation diagram of La/Nb vs. La/Ba for LPC rocks; OIB field after Fitton et al. (1991); Pleistocene-Holocene arc basalts field after Tormey et al. (1991); CVPM field is for the basalts and trachybasalts from Payún Matrú (Hernando et al., 2014). D) Covariation diagram of Th/Yb vs. Ta/Yb (Pearce, 1983). The LPC rocks plot in the field of the Central Andean basalts. Data plotted in figures C and D correspond only to fine grained rocks and exclude the cumulate clinopyroxenite.

idiomorphic rims in K-feldspar and some amphibole crystals suggest equilibrium crystallization within phonolitic melts. The textural and compositional changes in these minerals indicate that they crystallized in a dynamic environment, reaching equilibrium in the magmatic reservoir before the emplacement of phonolitic dikes.

5.3. Crustal contamination

The isotopic data of Lucassen et al. (2007) and Zappettini et al. (2013) show higher $^{87}Sr/^{86}Sr$ with increasing SiO_2 contents, from clinopyroxenite (0.70363–0.70396) and malignite (0.70379–0.70391) to syenites (0.704458–0.704577) and trachyte (0.705471). This change, plus Nd and Pb isotopic ratios, led Lucassen et al. (2007) to interpret mixing of melts from a depleted lithospheric mantle with small quantities of a different isotopic material. This contaminant must have non-radiogenic Nd and radiogenic Sr to produce the isotopic ratios shown by syenites. A reasonable candidate is the lower continental crust with a composition similar to that of the xenoliths hosted in a near volcanic neck in Precordillera studied by Kay et al. (1996).

We suggest, therefore, that the LPC is the result of fractional crystallization of an already evolved tephritic magma, that produced a clinopyroxenite cumulate plus malignite derivatives. The syenite is the result of further evolution but from magma that had become contaminated (AFC process), raising substantially the

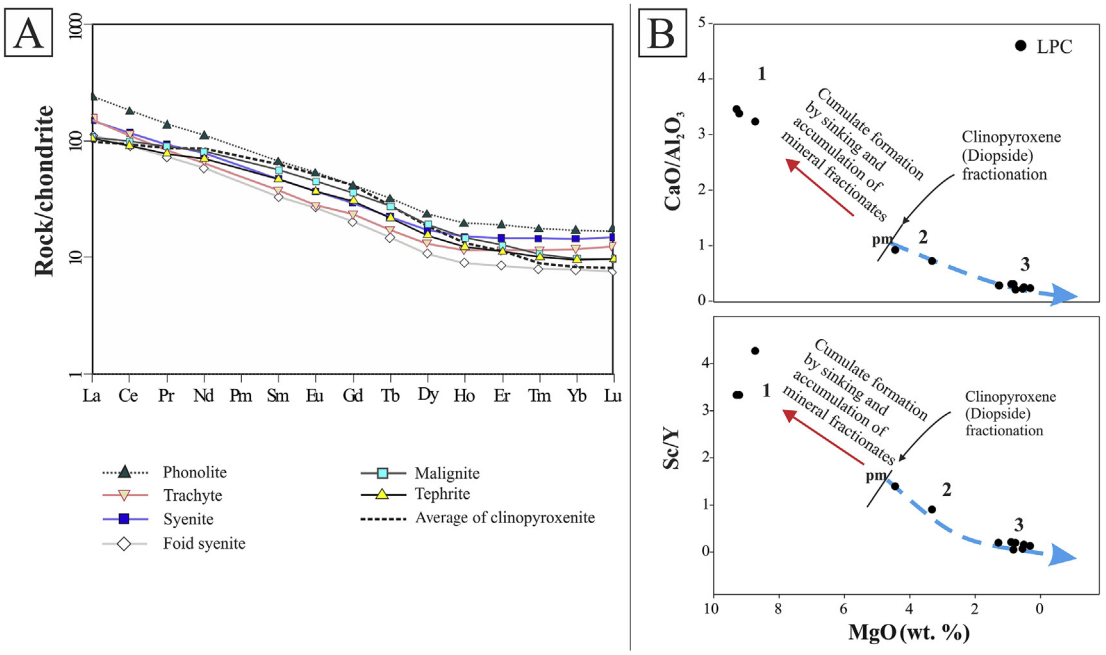

Fig. 12. A) REE diagram from LPC rocks normalized to chondrite after Boynton (1984). B) Covariation diagrams for MgO vs. CaO/Al_2O_3 and MgO vs. Sc/Y for LPC rocks. The positive correlation is controlled by clinopyroxene fractionation. Note the high MgO, CaO and Sc/Y values for cumulate rocks. 1, 2 and 3: rock group number; pm: parental magma (tephritic).

Table 11
Theoretical parental magmas calculated with mass-balance fractionation model, compared with tephritic dikes.

FC = 19%	MgO	SiO_2	TiO_2	Al_2O_3	Fe_2O_3t	MnO	CaO	Na_2O	K_2O	P_2O_5	Total	$\Sigma(r^2)$
Tephritic dike LPD32	4.66	45.09	1.71	13.57	14.29	0.25	12.73	2.15	4.15	1.40	100.0	
Theoretical parental (1)	4.66	45.03	1.70	12.95	14.32	0.23	12.89	2.40	4.58	1.24	100.0	0.68
Theoretical parental (2)	4.57	45.06	1.67	13.20	14.10	0.25	13.06	2.39	4.57	1.12	100.0	0.61
Theoretical parental (3)	4.53	45.36	1.67	13.38	13.82	0.25	12.83	2.42	4.69	1.06	100.0	0.84
Theoretical parental (4)	4.42	45.04	1.71	13.41	14.31	0.26	12.76	2.40	4.67	1.02	100.0	0.57

The theoretical parental magmas were calculated assuming a 19% of fractional crystallization (FC). In the model, malignite was considered as differentiated residual magma and the clinopyroxenite as solid waste (cumulate).
(1): Theoretical parental magma, calculated with a theoretical cumulate, formed by 70% of clinopyroxene (diopside), 23% of titanian magnetite and 7% of fluorapatite, giving a modal composition equivalent to the clinopyroxenite of the LPC. The chemical compositions of minerals used in this calculation correspond to LP12Cpx1 (Table 2), LP12Ap1 (Table 7) samples, and for magnetite, we used the analyses from tephritic dikes (see average compositions in the text).
(2), (3) and (4): Theoretical parental magmas, calculated with the real chemical compositions of different samples of clinopyroxenite. For (2) LP PX was used (Zappettini et al., 2013, Table 3). For (3) and (4) the LP12a and LP12c samples were used respectively (Table 9). For the calculations, chemical compositions (minerals and rocks) were recalculated to 100%. Note that the theoretical parental magmas have similar compositions to the tephritic dikes (sample LPD32 Table 9).

$^{87}Sr/^{86}Sr$ isotopic ratio. It is currently not possible to ascertain whether the same magma batch that produced the clinopyroxenite and malignite also gave origin to syenite and related rocks or not. We consider it more likely that they represent different batches, and that what is currently seen as a continuous evolution in Harker and related diagrams are in fact parallel (overlapping) liquid lines of descent of magmas, that started as basanitic and interacted in different degree with crustal materials.

5.4. The miocene magmatism in the region

The LPC is the easternmost occurrence of a group disposed along a NNW-SSE strike (Fig. 1B). The calc-alkaline andesites and monzodiorites of the Cerro Colorado and Paramillos de Uspallata volcanic centers, dated at 18.9–16.2 Ma (Kay et al., 1991), are located at approximately 15 km. Geochemical data from Carrasquero (2005) and Carrasquero et al. (2011) for Paramillos de Uspallata rocks show high SiO_2 contents (59.95–66.53 wt.%), very low MgO (0.11–0.96 wt.%) and medium to high alkali contents (9.15–10.03 wt.%). Based in the low Y and Yb values and the high Sr/Y and La/Yb ratios (>50 and > 20 respectively), these authors interpret that these magmas have a clear adakitic signature and would have formed by partial melting of a thicker mafic crust in equilibrium with garnet and amphibole. Besides, they show that these rocks have a trace element pattern typical of convergent plates and show incompatible elements enrichment (LILE and LREE) and strong negative anomalies of Nb, P and Ti. Based on Sr and Nd isotopes they suggest a depleted mantle source.

The Paramillos de Uspallata rocks with calc-alkaline affinity are distinctly different from those of the LPC. However, they share a similar pattern in the trace element patterns (Fig. 11B). The potassic silica subsaturated filiation, as well as the low La/Yb ratio, high Y contents and the absence of an adakitic signature in the LPC, suggest compositional differences in the source compared to Paramillos de Uspallata, possibly different depth of origin and different degrees of crustal contamination or alternatively different degrees of partial melting. Giambiagi et al. (2011) divided the Precordillera in two different structural domains (East and West), starting in a disruption zone called Villavicencio system faults. Based on the contrasting structural attitude of both domains, Giambiagi et al. (2014) inferred that this system is a suture between the Chilenia and Cuyania terranes. Differences in the crust composition must

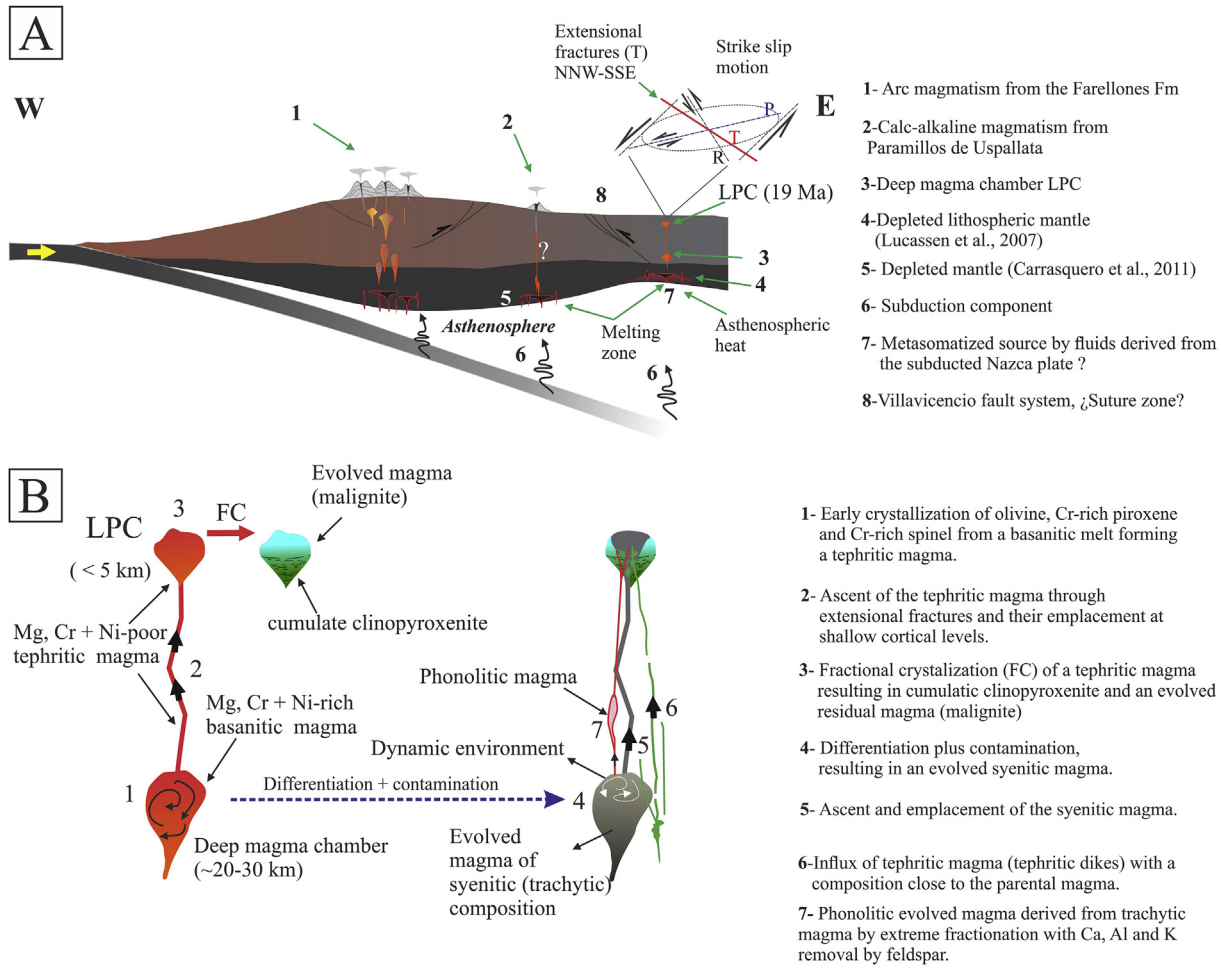

Fig. 13. A) Schematic representation of the geodynamic and magmatic conditions in the region (transect to 32° 41′S) for the Early Miocene age (20–16 Ma). B) Simplified magmatic evolution of the LPC.

have some influence, as it is considered that the mantle of the entire region was regenerated in the Cretaceous (Lucassen et al., 2007), although this is impossible to know without more data. Isotopic signatures observed in a sample of the Paramillos de Uspallata (data from Carrasquero et al., 2011), indicate a higher degree of crustal contamination compared to the LPC rocks.

The schematic representation of the geodynamic and magmatic conditions in the region, and the simplified magmatic evolutions of LPC are shown in Fig. 13.

5.5. The LPC compared to the alkaline magmatism from the Alto Paranaiba Igneus Province

The most voluminous alkaline magmatic occurrences of South America occur in the central–southeastern Brazil, known as the Alto Paranaiba Igneus Province (APIP) (Almeida, 1983; Gibson et al., 1995). The Late-Cretaceous APIP comprises ultrapotassic magmatism interpreted as the result of the initial impact of the Trindade mantle plume under the lithosphere of central Brazil, which acted as a heat source for the melting of the overlying subcontinental lithospheric mantle (Gibson et al., 1995). The APIP is composed of kamafugites and subordinated amounts of kimberlites, and rare lamproites (e.g., Araújo et al., 2001; Gibson et al., 1995). A number of large ultramafic cumulates, syenitic carbonatite- and phoscorite-bearing alkaline complexes occur in the APIP, comprising Catalão I and II, Serra Negra, Salitre I, II, and III, Araxá, and Tapira (Gomes et al., 1990; Morbidelli et al., 1997; Traversa et al., 2001; Brod et al., 2004). The APIP rocks with ultrapotassic affinity are strongly different from those of the LPC; however, some petrographic similarities are recognized, principally in the ultramafic silicate rocks. Clinopyroxenite from La Peña complex are mineralogically and petrographically similar to the more evolved clinopyroxenite (bebedorites) from APIP complexes (see Brod et al., 2005; Barbosa et al., 2012) but the geochemical data of these bebedorites, for example for Salitre I complex (Barbosa et al., 2012) show a trace element pattern typical of within plate geodynamic setting and strong LREE enrichment compared to those from LPC.

The LPC rocks compared to APIP magmatism, show: 1) potassic and not ultrapotassic affiliation, 2) absence of rocks with carbonatitic, phoscoritic, lamproitic and kamafugitic affinity, and 3) trace elements behavior typical of magmas related to subduction. The LPC and the APIP are examples of alkaline magmatism of the potassic series developed in contrasting tectonic setting, which is clearly reflected in the trace element pattern.

6. Conclusions

The LPC is a potassic, silica-subsaturated magmatic complex emplaced during the Miocene in the Precordillera, that was originated by a parental tephritic melts that have possibly already undergone olivine, clinopyroxene and spinel segregation from the primary or primitive mantle-derived magma originated from

partial melting in an initially depleted and later enriched lithospheric mantle source.

Our model proposes that the parental melts with an arc signature were emplaced in the upper crust (<5 km). The first magma batch differentiated *in situ* in a clinopyroxenite cumulate leaving a residual magma that crystallized as malignite. Additional fractional crystallization in the deep magma chamber, possibly combined with rock assimilation (AFC), originated more evolved melts that were emplaced in successive batches that formed the syenitic-trachytic units and more alkaline dikes. Trends of mineral and whole rock compositions attest for this evolution. Recharge events with local mingling and mixing between tephrites and trachytes-phonolite magmas had occurred at the end of the LPC evolution. The textural and compositional changes in K-feldspar and amphibole from phonolite, suggest a dynamic environment of crystallization, meanwhile the idiomorphic outer zone of these phases suggest late–stage equilibrium crystallization within phonolitic melt in a deeper magmatic reservoir before the emplacement of phonolitic dikes.

The intrusive process was facilitated by the opening of extensional NNW-SSE fractures genetically linked to a local brittle shear zone, active at 18–19 Ma during a strong compressional event that initiated the regime of flat-slab subduction in this part of the Andes.

The LPC rocks show similar trace element patterns to other Miocene magmatic manifestations related to subduction. However, the LPC rocks have a clearly different composition that suggests the involvement of different sources, different degrees of crustal contamination, different degrees of partial melting or alternatively different depths of melt generation for the Miocene magmatism in the region.

Acknowledgments

This study was made possible by the support of CONICET (Argentina) through the grant PIP 11220090100857. The authors are grateful for the thorough reviews of the manuscript by P. Caffe and an anonymous reviewer as well as for the editorial suggestions and corrections made by the Editor-in-Chief J. Kellogg. The authors are very grateful to A. Guereschi for her help with the electron microprobe, and to F. Martina and P. Cordenons for their suggestions related to the geochemical and petrologic interpretations.

References

Almeida, F.F.M., 1983. Relações tectônicas das rochas alcalinas mesozóicas da região meridional da Plataforma Sul-Americana. Rev. Bras. Geociências 13, 139–158.
Araújo, A.L.N., Carlson, R.W., Gaspar, J.C., Bizzi, L.A., 2001. Petrology of kamafugites and kimberlites from the Alto paranaíba alkaline province, minas Gerais, Brazil. Contributions Mineralogy Petrology 142, 163–177.
Baier, J., Audétat, A., Keppler, H., 2008. The origin of the negative niobium tantalum anomaly in subduction zone magmas. Earth Planet. Sci. Lett. 267, 290–300.
Bailey, D.K., Schairer, J.F., 1964. Feldspar-liquid equilibria in peralkaline liquids; the orthoclase effect. Am. J. Sci. 262 (10), 1198–1206.
Barbosa, E.S.R., Brod, J.A., Junqueira-Brod, T.C., Dantas, E.L., Cordeiro, P.F.D.O., Gomide, C.S., 2012. Bebedourite from its type area (Salitre I complex): a key petrogenetic series in the Late-Cretaceous Alto Paranaíba kamafugite-carbonatite- phoscorite association, Central Brazil. Lithos 144, 56–72.
Blancher, S.B., D'Arco, P., Fonteilles, M., Pascal, M.L., 2010. Evolution of nepheline from mafic to highly differentiated members of the alkaline series: the Messum complex, Namibia. Mineral. Mag. 74 (3), 415–432.
Boari, E., Tommasini, S., Laurenzi, M.A., Conticelli, S., 2009. Transition from ultrapotassic kamafugitic to sub-alkaline magmas: Sr, Nd, and Pb isotope, trace element and 40Ar–39Ar age data from the Middle Latin Valley volcanic field, Roman Magmatic Province, Central Italy. J. Petrol. 00, 1–31.
Bowen, N.L., 1945. Phase equilibria bearing on the origin and differentiation of alkaline rocks. Am. J. Sci. 243, 75–89.
Boynton, W.V., 1984. Cosmochemistry of the rare earth elements: meteorite studies. In: Henderson, P. (Ed.), Rare Earth Element Geochemistry. Elsevier, Amsterdam, pp. 63–114.
Brod, J.A., Gaspar, J.C., Araújo, D.P., Gibson, S.A., Thompson, R.N., Junqueira-Brod, T.C., 2001. Phlogopite and tetra-ferriphlogopite from Brazilian carbonatite complexes: petrogenetic constraints and implications for mineral-chemistry systematics. J. Asian Earth Sci. 19, 265–296.
Brod, J.A., Ribeiro, C.C., Gaspar, J.C., Junqueira-Brod, T.C., Barbosa, E.S.R., Riffel, B.F., Silva, J.F., Chaban, N., Ferrari, A.J.D., 2004. 42 Congresso Brasileiro de Geologia. Geologia e Mineralizações dos Complexos Alcalino-Carbonatíticos da Província Ígnea do Alto Paranaíba. In: Field Trip Guide, p. 29.
Brod, J.A., Gaspar, J.C., Diniz-Pinto, H.S., Junqueira-Brod, T.C., 2005. Spinel chemistry and petrogenetic processes in the Tapira alkaline–carbonatite complex, Minas Gerais, Brazil. Rev. Bras. Geociências 35, 23–32.
Broderick, C.A., 2008. The Origin of Sulfur-rich Apatites in Silicic Magmas. Master's thesis. Portland State Univ. Portland, OR, USA.
Cahill, T., Isacks, B., 1992. Seismicity and shape of the subducted Nazca plate. J. Geophys. Res. 97, 17503–17529.
Carrasquero, S.I., 2005. Petrology and Geochemistry Data of Miocene Volcanism of Paramillos de Uspallata, Argentina. In: Geophysical Research Abstracts, p. 7.
Carrasquero, S.I., Rubinstein, N.A., Fontignie, D., 2011. Adakite-like signature in volcanic rocks associated with the Oro del Sur Au-(Cu) epithermal deposit, Southern Precordillera, Argentina. Geol. Paläontologie Abh. 261 (3), 309–320.
Charrier, R., Baeza, O., Elgueta, S., Flynn, J.J., Gans, P., Kay, S.M., Muñoz, N., Wyss, A.R., Zurita, E., 2002. Evidence for Cenozoic extensional basin development and tectonic inversion in the southern Central Andes, Chile (33° 36° S.L.). J. S. Am. Earth Sci. 15 (1), 117–139.
Charrier, R., Bustamante, M., Comte, D., Elgueta, S., Flynn, J.J., Iturra, N., Muñoz, N., Pardo, M., Thiele, R., Wyss, A.R., 2005. The Abanico extensional basin: regional extension, chronology of tectonic inversion, and relation to shallow seismic activity and Andean uplift. Neues Jahrb. für Geol. Paläontologie Abh. 236 (1–2), 43–77.
Coulson, I.M., Russell, J.K., Dipple, G.M., 1999. Origins of the Zippa Mountain pluton: a late triassic, arc-derived, ultrapotassic magma from the Canadian Cordillera. Can. J. Earth Sci. 36 (9), 1415–1434.
Cuerda, A., Cingolani, C., Bordonaro, O., 1993. Las secuencias sedimentarias eopaleozoicas. In: Ramos, V.A. (Ed.), Geología y Recursos Naturales de Mendoza, Congreso Geológico Argentino y Congreso de Exploración de Hidrocarburos, Relatorio, Mendoza, Asociación Geológica Argentina, vol. 1, pp. 21–30 (Buenos Aires).
Davis, J.S., Roeske, S.M., McClelland, W., Kay, S.M., 2000. Mafic and ultramafic crustal fragments of the southwestern Precordillera terrane and their bearing on tectonic models of the early Paleozoic in western Argentina. Geology 28, 171–174.
Droop, G.T.R., 1987. A general equation for estimating Fe^{3+} concentrations in ferromagnesian silicates and oxides from microprobe analyses, using stoichiometric criteria. Min. Mag. 51, 431–435.
Edwards, C.M.H., Menzies, M.A., Thirlwall, M.F., Morris, J.D., Leeman, W.P., Harmon, R.S., 1994. The transition to potassic alkaline volcanism in island arcs: the Ringgit-Beser complex, East Java, Indonesia. J. Petrol. 35, 1557–1595.
Fitton, J.G., James, D., Leeman, W.P., 1991. Basic magmatism associated with Late Cenozoic extension in the Western United States: compositional variations in space and time. J. Geophys. Res. 96 (B8), 13693–13711.
Flohr, M.J.K., Ross, M., 1990. Alkaline igneous rocks of Magnet cove, Arkansas: mineralogy and geochemistry of syenites. Lithos 26, 67–98.
Fock, A., 2005. Cronología y tectónica de la exhumación en el Neógeno de los Andes de Chile central entre los 33°y los 34°S. Master Thesis. Universidad de Chile, Chile.
Foley, S.F., Venturelli, G., Green, D.H., Toscani, L., 1987. The ultrapotassic rocks: characteristics, classification and constraints for petrogenetic models. Earth Sci. Rev. 24, 81–134.
Giambiagi, L., Mescua, J., Bechis, F., Martínez, A., Folguera, A., 2011. Pre-Andean deformation of the Precordillera southern sector, southern Central Andes. Geosphere 7, 219–239.
Giambiagi, L., Mescua, J., Heredia, N., Farías, P., García Sansegundo, J., Fernández, C., Stier, S., Pérez, D., Bechis, F., Moreiras, S.M., Lossada, A., 2014. Reactivation of Paleozoic structures during Cenozoic deformation in the Cordón del Plata and Southern Precordillera ranges (Mendoza, Argentina). J. Iber. Geol. 40 (2), 309–320.
Gibson, S.A., Thompson, R.N., Leonardos, O.H., Dickin, A.P., Mitchell, J.G., 1995. The Late Cretaceous impact of the Trindade mantle plume evidence from large volume, mafic, potassic magmatism in SE Brazil. J. Petrol. 36, 189–229.
Gomes, C.B., Ruberti, E., Morbidelli, L., 1990. Carbonatite complexes from Brazil: a review. J. S. Am. Earth Sci. 3, 51–63.
Hamilton, D.L., 1961. Nephelines as crystallization temperature indicators. J. Geol. 69, 321–329.
Harrington, H.J., 1941. Investigaciones geológicas en las sierras de Villavicencio y Mal País, Provincia de Mendoza. Dirección Minería Geol. 49, 54.
Hawthorne, F.C., Oberti, R., Harlow, G.E., Maresch, W.V., Martin, R.F., Schumacher, J.C., Welch, M.D., 2012. Nomenclature of the amphibole supergroup. Am. Mineral. 97 (11–12), 2031–2048.
Henderson, C.M.B., Gibb, F.G.F., 1983. Felsic mineral crystallization trends in differentiating alkaline basic magmas. Contrib. Mineral. Petrol. 84, 355–364.
Hernando, I.R., Aragón, E., Frei, R., González, P.D., Spakman, W., 2014. Constraints on the origin and evolution of magmas in the Payún Matrú volcanic field, quaternary andean back-arc of western Argentina. J. Petrol. 55 (1), 209–239.
Hickey, R.L., Frey, F.A., Gerlach, D.C., 1986. Multiple sources for basaltic arc rocks from the southern volcanic zone of the Andes (34°- 41°S): trace element and isotopic evidence for contributions from subducted oceanic crust, mantle, and continental crust. J. Geophys. Res. 91, 5963–5983.

Irvine, T.N., Baragar, W.R.A., 1971. A guide to the chemical classification of the common volcanic rocks. Can. J. Earth Sci. 8, 523–548.
Kay, S., Mpodozis, C., 2001. Central Andean ore deposits linked to evolving shallow subduction systems and thickening crust. Geol. Soc. Am. Today 11, 4–9.
Kay, S.M., Mpodozis, C., 2002. Magmatism as a probe to the Neogene shallowing of the Nazca plate beneath the modern Chilean flat-slab. J. S. Am. Earth Sci. 15, 39–57.
Kay, S.M., Maksaev, V., Moscoso, R., Mpodozis, C., Nasi, C., 1987. Probing the evolving Andean lithosphere: mid-late Tertiary magmatism in Chile (29°–30°30′S) over the modern zone of subhorizontal subduction. J. Geophys. Res. 92, 6173–6189.
Kay, S.M., Godoy, E., Kurtz, A., 2005. Episodic arc migration, crustal thickening, subduction erosion, and magmatism in the south-central Andes. Geol. Soc. Am. Bull. 117, 67–88.
Kay, S.M., Burns, M., Copeland, P., Mancilla, O., 2006. Upper Cretaceous to Holocene magmatism and evidence for transient Miocene shallowing of the Andean subduction zone under the northern Neuquén Basin. In: Kay, S.M., Ramos, V.A. (Eds.), Evolution of an Andean Margin: a Tectonic and Magmatic View from the Andes to the Neuquén Basin (35°-39°S Lat). Boulder, Colorado, Geological Society of America Special Paper. 407, pp. 19–60.
Kay, S.M., Mpodozis, C., Coira, B., 1999. Neogene magmatism, tectonism, and mineral deposits of the Central Andes (22°-33°S latitude). In: Skinner, B.J. (Ed.), Geology and Ore Deposits of the Central Andes, Society of Economic Geologists, Special Publication, vol. 7, pp. 27–59.
Kay, S.M., Mpodozis, C., Ramos, V.A., Munizaga, F., 1991. Magma source variations for mid-late tertiary magmatic rocks associated with a shallowing subduction zone and a thickening crust in the Central Andes (28 to 33°S). In: Harmon, R.S., Rapela, C.W. (Eds.), Andean Magmatism and its Tectonic Setting, Geological Society of America Special Paper, 265, pp. 113–137.
Kay, S.M., Orrell, S., Abbruzzi, J.M., 1996. Zircon and whole rock Nd–Pb evidence for a Grenville age and a Laurentian origin for the basement of the Precordillera in Argentina. J. Geol. 104, 637–648.
Kogarko, L.N., Kononova, V.A., Orlova, M.P., Woolley, A.R., 1995. Alkaline Rocks and Carbonatites of the World: Part 2. Former USSR. Chapman and Hall, London, p. 225.
Kononova, V.A., Organova, N.I., Lomeyko, Y.I., 1967. Composition and crystalline temperature of nepheline from rocks of an ijolite-melteigite series. Int. Geol. Rev. 9 (9), 1229–1236.
Larsen, L.M., 1976. Clinopyroxenes and coexisting mafic minerals from the alkaline Ilimaussaq intrusion, South Greenland. J. Petrol. 17, 258–290.
Le Bas, M.J., 1977. Carbonatite and Nephelinite Volcanism. An African Case History. Wiley, London, p. 347.
Le Bas, M.J., Le Maitre, R.W., Streckeisen, A., Zanettin, B., 1986. A chemical classification of volcanic rocks based on the total alkali-silica diagram. J. Petrol. 27 (3), 745–750.
Le Maitre, R.W., 2002. Igneous Rocks: a Classification and Glossary of Terms: Recommendations of the International Union of Geological Sciences Subcommission on the Systematics of Igneous Rocks. Cambridge University Press, Cambridge.
Lucassen, F., Franz, G., Romer, R.L., Schultz, F., Dulski, P., Wemmer, K., 2007. Pre-Cenozoic intra-plate magmatism along the Central Andes (17-34°S): composition of the mantle at an active margin. Lithos 99, 312–338.
Mattsson, H., Oskarsson, N., 2005. Petrogenesis of alkaline basalts at the tip of a propagating rift: evidence from the Heimaey volcanic centre, south Iceland. J. Volcanol. Geotherm. Res. 147, 245–267.
Maydagán, L., Franchini, M., Chiaradia, M., Pons, J., Impiccini, A., Toohey, J., Rey, R., 2011. Petrology of the Miocene igneous rocks in the Altar region, main Cordillera of San Juan, Argentina. A geodynamic model within the context of the Andean flat-slab segment and metallogenesis. J. S. Am. Earth Sci. 32 (1), 30–48.
Miller, C., Schuster, R., Klötzli, U., Frank, W., Purtscheller, F., 1999. Post-collisional potassic and ultrapotassic magmatism in SW Tibet: geochemical and Sr–Nd–Pb–O isotopic constraints for mantle source characteristics and petrogenesis. J. Petrol. 40 (9), 1399–1424.
Mitchell, R.H., 1996. Undersaturated alkaline rocks: mineralogy, petrogenesis, and economic potential. Mineral. Assoc. Can. 24.
Mitchell, R.H., Platt, R.G., 1979. Nepheline-bearing rocks from the poohbah Lake complex, Ontario: malignites and malignites. Contrib. Mineral. Petrol. 69, 255–264.
Mitchell, R.H., Platt, R.G., 1982. Mineralogy and petrology of nepheline syenites from the Coldwell alkaline complex, Ontario, Canada. J. Petrol. 23 (2), 186–214.
Morbidelli, L., Gomes, C.B., Beccaluva, L., Brotzu, P., Conte, A.M., Ruberti, E., Traversa, G., 1995. Mineralogical, petrological and geochemical aspects of alkaline and alkaline-carbonatite associations from Brazil. Earth Sci. Rev. 39 (3), 135–168.
Morbidelli, L., Gomes, C.B., Beccaluva, L., Brotzu, P., Garbarino, C., Riffel, B.F., Ruberti, E., Traversa, G., 1997. Parental magma characterization of Salitre cumulate rocks (Alto Paranaíba Alkaline Province, Brazil) as inferred from mineralogical, petrographic, and geochemical data. Int. Geol. Rev. 39, 723–743.
Morimoto, N., Fabries, J., Ferguson, A.K., Ginzburg, I.V., Ross, M., Seifert, F.A., Zussman, Aoki, K., Gottardi, G., 1988. Nomenclature of pyroxenes. Am. Mineral. 73, 1123–1133.
Oberti, R., Cannillo, E., Toscani, G., 2012. How to name amphiboles after the IMA2012 report: rules of thumb and a new PC program for monoclinic amphiboles. Period. Mineral. 81 (2), 257–267.
Pagano, D.S., Galliski, M.A., Márquez-Zavalía, M.F., 2014. Emplacement of the La Peña alkaline igneous complex, Mendoza, Argentina (33° S): implications for the early Miocene tectonic regime in the retroarc of the Andes. J. S. Am. Earth Sci. 50, 48–66.
Pearce, J.A., 1982. Trace element characteristics of lavas from destructive plate boundaries. In: Thorpe, R.S. (Ed.), Andesites. John Wiley, pp. 525–548.
Pearce, J.A., 1983. Role of the sub-continental lithosphere in magma genesis at active continental margins. In: Hawkesworth, C.J., Norry, M.J. (Eds.), Continental Basalts and Mantle Xenoliths. Shiva, pp. 230–249.
Pearce, J.A., 1996. A user's guide to basalt discrimination diagrams. In: Wyman, D.A. (Ed.), Trace Element Geochemistry of Volcanic Rocks: Applications for Massive Sulphide Exploration, Geological Association of Canada, Short Course Notes, vol. 12, pp. 79–113.
Reich, M., Parada, M.A., Palacios, C., Dietrich, A., Schultz, F., Lehmann, B., 2003. Adakite-like signature of Late Miocene intrusions at the Los Pelambres giant porphyry copper deposit in the Andes of central Chile: metallogenic implications. Miner. Deposita 38, 876–885.
Richards, J.P., Boyce, A.J., Pringle, M.S., 2001. Geological evolution of the Escondida area, northern Chile: a model for spatial and temporal localization of porphyry Cu mineralization. Econ. Geol. 96, 271–305.
Ridolfi, F., Renzulli, A., 2012. Calcic amphiboles in calc-alkaline and alkaline magmas: thermobarometric and chemometric empirical equations valid up to 1,130°C and 2.2 GPa. Contrib. Mineral. Petrol. 163, 877–895.
Ridolfi, F., Renzulli, A., Puerini, M., 2010. Stability and chemical equilibrium of amphibole in calc-alkaline magmas: an overview, new thermobarometric formulations and application to subduction-related volcanoes. Contrib. Mineral. Petrol. 160 (1), 45–66.
Rittmann, A., 1957. On the serial character of igneous rocks. Egypt. J. Geol. 1, 23–48.
Rudnick, R.L., Fountain, D.M., 1995. Nature and composition of the continental crust: a lower crustal perspective. Rev. Geophys. 33 (3), 267–309.
Skewes, A., Stern, C.R., 1994. Tectonic trigger for the formation of Late Miocene Curich breccia pipes in the Andes of central Chile. Geology 22, 551–554.
Stephenson, D., 1972. Alkali clinopyroxenes from nepheline syenite of the South Qoroq Centre, south Greenland. Lithos 5, 187–201.
Stern, C.R., 1989. Pliocene to present migration of the volcanic front, Andean southern volcanic front. Rev. Geol. Chile 16, 145–162.
Stern, C.R., Skewes, M.A., Arévalo, A., 2010. Magmatic evolution of the giant El Teniente Cu-Mo deposit, central Chile. J. Petrol. 52 (7–8), 1591–1617.
Sun, S.S., McDonough, W., 1989. Chemical and Isotopic Systematics of Oceanic Basalts: Implications for Mantle Composition and Processes. In: Geological Society, London, Special Publications, 42(1), pp. 313–345.
Tormey, D.R., Hickey-Vargas, R., Frey, F.A., López-Escobar, L., 1991. Recent lavas from the Andean volcanic front (33° to 42°S); Interpretations of along-arc compositional variations. In: Harmon, R.S., Rapela, C.W. (Eds.), Andean Magmatism and its Tectonic Setting, Geological Society of America, Special Papers, 265, pp. 57–77.
Traversa, G., Gomes, C.B., Brotzu, P., Buraglini, N., Morbidelli, L., Principato, M.S., Ronca, S., Ruberti, E., 2001. Petrography and mineral chemistry of carbonatites andmica-rich rocks from the Araxá complex (Alto Paranaíba Province, Brazil). An. Acad. Bras. Ciências 73, 71–98.
Vergara, M., Morata, D., Villarroel, R., Nyström, J., Aguirre, L., 1999. Ar/Ar ages, very low-grade metamorphism and geochemistry of the volcanic rocks from "Cerro El Abanico", Santiago Andean Cordillera (33°30'S-70° 30'-70° 25'W). In: Proceedings of the IV International Symposium on Andean Geodynamics, Göttingen, Germany, pp. 785–788.
Villar, L.M., Zappettini, E.O., 2000. El Complejo alcalino Paleógeno de Puesto La Peña. En: simposio Internacional Magmatismo Andino. In: Actas IX Congreso Geológico Chileno, 2, pp. 697–701.
Whitney, D.L., Evans, B.W., 2010. Abbreviations for names of rock-forming minerals. Am. Mineral. 95 (1), 185–187.
Wilkinson, J.F.G., Hensel, H.D., 1994. Nephelines and analcimes in some alkaline igneous rocks. Contrib. Mineral. Petrol. 118, 79–91.
Woolley, A.R., Platt, R.G., 1986. The mineralogy of nepheline syenite complexes from the northern part of the Chilwa Province, Malawi. Mineral. Mag. 50, 597–610.
Zappettini, E.O., Basei, M.A., Villar, L., Teixeira, W., 2005. Edad de la facies malignita del Complejo Alcalino Puesto La Peña, Mendoza, Argentina. In: Actas del XVI Congreso Geológico Argentino, Artículo, vol. 537, p. 6.
Zappettini, E.O., Brodtkorb, M.K., Bernhardt, H.-J., Villar, L., 2008. Sobre los espinelos del complejo alcalino Puesto La Peña, provincia de Mendoza. In: Actas XVII Congreso Geológico Argentino, Jujuy, 695.
Zappettini, E.O., Brodtkorb, M.K., de, Bernhardt, H.-J., Villar, L.M., 2009. Los espinelos del complejo alcalino Puesto La Peña, provincia de Mendoza. Rev. la Asoc. Geol. Argent. 64 (3), 544–549.
Zappettini, E.O., Villar, L.M., Hernández, L.B., Santos, J.O., 2013. Geochemical and isotopic constraints on the petrogenesis of the Puesto La Peña undersaturated potassic complex, Mendoza province, Argentina, geodynamic implications. Lithos 162–163, 301–316.